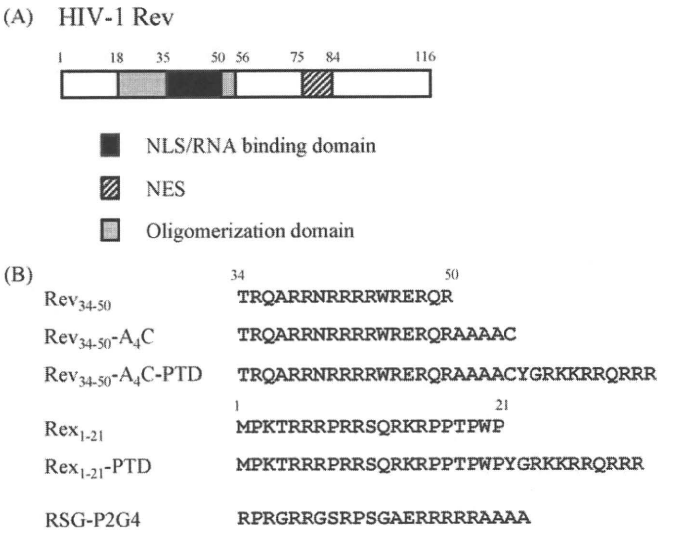

Fig. 1. Domain structure of HIV-1 Rev and sequences of Rev- and Rex-derived peptides. (A) Diagrammatic representation of HIV-1 Rev. The functional domains and regions of HIV-1 Rev are depicted. (B) Sequences of Rev-derived, Rex-derived and RSG-P2G4 peptides. The Rev- and Rex-derived peptides were synthesized based on the HIV-1_{NL4-3} (GenBank Accession No. AF324493) and HTLV-I MT-2 (GenBank Accession No. L03561) sequences, respectively. The protein transduction domain (PTD; YGRKKRRQRRR), an amino acid sequence derived from HIV-1_{NL4-3} Tat protein (aa 47–57), was added to the C-terminus of the peptides.

At least three properties seem to be required to antagonize Rev function: cell permeability, nuclear localization and specific binding to HIV-1 RRE or Rev. In this regard, Rev M10, a Rev mutant lacking the nuclear export activity, efficiently suppresses HIV-1 replication through a dominant-negative effect on Rev function (Malim et al., 1989a). However, it has several obstacles to overcome, such as immunogenicity, chemical synthesis and administration, for clinical application. In contrast, small peptides may be ideal for overcoming such obstacles. Harada et al. (1996, 1997) designed and examined artificial arginine-rich peptides as Rev antagonists in biochemical binding assays. The crystal structure of Rev/RRE has been reported (Jain and Belasco, 2001). Based on this structure (Jain and Belasco, 2001; Jiang et al., 1999), we designed peptides of 17 and 21 amino acids derived from the RRE-binding domains of Rev and Rex proteins, designated Rev_{34-50} and Rex_{1-21}, respectively, and examined their anti-HIV-1 activities. These peptides contain an arginine-rich domain, which not only binds to the RRE but also imparts cell permeability and nuclear localization (Futaki et al., 2001). Notably, it has been reported that arginine-rich peptides, e.g., ALX40-4C (N-α-acetyl-nona-D arginine), show anti-HIV-1 activity via antagonistic effects against CXCR4 (Doranz et al., 1997). We hypothesized that the arginine-rich RNA-binding domains of Rev and Rex inhibit both the entry of HIV-1 through CXCR4 and the production of progenitor HIV-1 by interrupting the function of Rev in the early and late phases of the replication cycle.

In this study, we tested this hypothesis by synthesizing Rev- and Rex-derived peptides based on their RNA-binding domains, as well as RSG-P2G4, an arginine-rich peptide that interacts with the RRE (Harada et al., 1997), and by evaluating their antiviral activities as bifunctional inhibitors that target Rev and CXCR4.

2. Materials and methods

2.1. Reagents

AZT was purchased from Sigma (St. Louis, MO). Amprenavir (APV) was kindly provided by Dr. H. Mitsuya (Kumamoto University, Kumamoto, Japan). AMD3100 was a kind gift from Dr. S. Shigeta (Fukushima Medical University, Fukushima, Japan). TAK-779 was obtained from the AIDS Research and Reference Program, Division of AIDS, National Institute of Allergy and Infectious Disease (Bethesda, MD). All peptides used in this study were chemically synthesized by Fmoc-solid-phase peptide synthesis on a Rink amide resin as reported previously (Futaki et al., 1997). A phycoerythrin (PE)-conjugated mouse anti-human CXCR4 MAb (12G5) was purchased from BD Bioscience Clontech (San Jose, CA).

2.2. Cells and viruses

Two laboratory strains, HIV-1_{IIIB} and HIV-1_{Ba-L}, that mainly interact with CXCR4 and CCR5 as coreceptors, respectively, were used in this study.

MT-2 cells were grown in RPMI 1640 medium (Sigma, St. Louis, MO). PM1-CCR5 cells, which are CCR5-transduced PM1 cells, and PM1-CCR5/IIIB and PM1-CCR5/Ba-L cells, which are PM1-CCR5 cells persistently infected with HIV-1_{IIIB} or HIV-1_{Ba-L}, respectively, were maintained in RPMI 1640 medium supplemented with G418 disulfide (0.5 mg/ml; Nacalai Tesque, Kyoto, Japan). HeLa CD4/CCR5/LTR-β-galactosidase (MAGI/CCR5) cells (Vodicka et al., 1997) were kindly provided by Dr. J. Overbaugh through the AIDS Research and Reference Program. MAGI/CCR5, 293T and NP-2 cells were maintained in Dulbecco's modified Eagle's medium (Sigma). All media were supplemented with 10% fetal calf serum (FCS), 2 mM L-glutamine, 100 U/ml penicillin and 50 μg/ml streptomycin.

2.3. Determination of anti-HIV-1 activity

The anti-HIV-1 activities of the peptides in the early phase of the replication cycle were determined by the MAGI assay as described previously (Nameki et al., 2005). The inhibitory effects of the peptides in the late phase were evaluated using PM1-CCR5 cells persistently infected with HIV-1. Briefly, PM1-CCR5/IIIB or PM1-CCR5/Ba-L cells were washed three times and resuspended at 4×10^4 cells/ml with the peptides in the RPMI 1640-based medium. After 48 h, the amounts of viral p24 antigen present in the culture supernatants were measured using a RETRO-TEK HIV-1 p24 Antigen ELISA Kit (ZeptoMetrix Corporation, Buffalo, NY). The cytotoxicities of the peptides were evaluated by a 3-(4,5-dimethylthiazol-2-yl)-2,5-diphenyltetrazolium bromide (MTT) colorimetric assay as described previously (Kodama et al., 2001).

2.4. Flow cytometric analysis of the antagonistic effects on CXCR4

MT-2 cells were resuspended in phosphate-buffered saline (PBS) containing 1% FCS and preincubated with peptides at 4 °C for 30 min. PE-conjugated anti-CXCR4 MAb (12G5) was then added and incubated at 4 °C for a further 30 min. The cells were washed three times, fixed with 1% formaldehyde and analyzed using an EPICS XL flow cytometer (Beckman Coulter, Miami Lakes, FL).

2.5. Evaluation of the anti-HIV-1 effects of intracellular expression of Rev peptides

We constructed pCI-Rev-IG vectors encoding various Rev mutants, an internal ribosomal entry site (IRES) and neomycin phosphotransferase ($G418^r$) under the control of a cytomegalovirus (CMV) promoter as shown in Fig. 4. The pCI-Rev-IG plasmids were transfected into MT-2 cells using the TransIT transfection reagent (Mirus Bio, Madison, WI). After 16 h, the transduced MT-2 cells were subjected to G418 selection, and further cultured in the presence of G418 (0.5 mg/ml).

Rev-transduced MT-2 cells were resuspended in 96-well plates (3×10^3 cells/well) and incubated with HIV-1_{IIIB}. After 5 days, the

cytopathic effects were determined by the MTT assay as described previously (Kodama et al., 2001).

2.6. Subcellular localizations of Rev and Rex peptides

To evaluate the subcellular localizations of Rev and Rex peptides, we constructed $pRev_{peptide}$-EGFP and $pRex_{peptide}$-EGFP vectors expressing C-terminally EGFP-fused peptides using pEGFP N1 (Clontech Laboratories Inc., Palo Alto, CA). The plasmids were transfected into 293T and NP-2 cells using the TransIT transfection reagent. After 48 h, the cells were fixed with 1% formaldehyde and examined with a BioZERO fluorescence microscope (BZ-8000; Keyence, Osaka, Japan).

3. Results

3.1. Arginine-rich peptides inhibit HIV-1_{IIIB} infection

The amino acid sequences of the peptides are shown in Fig. 1. The peptides were examined for their anti-HIV-1 activities by the MAGI assay (Table 1), which only detects anti-HIV-1 activity in the early phase of the replication cycle up to the point of Tat interaction with the long terminal repeat (LTR) within 48 h post viral inoculation (Uchida et al., 1997). The reverse transcriptase inhibitor zidovudine (AZT) inhibited both HIV-1_{IIIB} and HIV-$1_{Ba\text{-}L}$, which use CXCR4 and CCR5 as coreceptors, respectively, while AMD3100 and TAK-779, which are specific antagonists of CXCR4 or CCR5 (Baba et al., 1999; Donzella et al., 1998), only inhibited HIV-1_{IIIB} and HIV-$1_{Ba\text{-}L}$, respectively. All peptides showed anti-HIV-1 activity against HIV-1_{IIIB}, but not HIV-$1_{Ba\text{-}L}$. Addition of the 5 amino acids AAAAC (A_4C), which stabilizes the α-helical structure (Lin et al., 2004), to the C-terminus of $Rev_{34\text{-}50}$ ($Rev_{34\text{-}50}$-A_4C) enhanced the activity against HIV-1_{IIIB} compared with the parental $Rev_{34\text{-}50}$. The anti-HIV-1 activity of $Rev_{34\text{-}50}$-A_4C was slightly enhanced by addition of the protein transduction domain of HIV-1 Tat (Tat-PTD) to the C-terminus (see Fig. 1B), which increases the intracellular delivery of the conjugated protein or peptide (Nagahara et al., 1998). $Rex_{1\text{-}21}$ partially inhibited infection by HIV-1_{IIIB} at 10 μM (approximately 40%) and its anti-HIV-1 activity was increased by addition of Tat-PTD. Another arginine-rich peptide, RSG-P2G4 (Harada et al., 1997), also only inhibited HIV-1_{IIIB} infection.

Table 1
Anti-HIV-1 activities of Rev- and Rex-derived peptides[a].

Compound	EC_{50}[b] (μM)	
	HIV-1_{IIIB}	HIV-$1_{Ba\text{-}L}$
$Rev_{34\text{-}50}$	1.7 ± 0.25	>10
$Rev_{34\text{-}50}$-A_4C	0.35 ± 0.07	>10
$Rev_{34\text{-}50}$-A_4C-PTD	0.37 ± 0.09	>10
$Rex_{1\text{-}21}$	>10	>10
$Rex_{1\text{-}21}$-PTD	2.5 ± 0.76	>10
RSG-P2G4	2.2 ± 0.51	>10
AZT	0.022 ± 0.005	0.055 ± 0.009
AMD3100	0.0038 ± 0.0011	>100
TAK-779	>100	0.0030 ± 0.0019

[a] Anti-HIV-1 activity was determined by the MAGI assay that detects early phase of HIV replication (Uchida et al., 1997). HIV-1_{IIIB} and HIV-$1_{Ba\text{-}L}$ are one of representative strains for CXCR4 and CCR5 tropic HIV-1.

[b] EC_{50}, 50% effective concentration. Data represent the means ± SD of at least three independent experiments.

3.2. Antagonism against CXCR4

It has been demonstrated that arginine-rich peptides bind to CXCR4, resulting in inhibitory effects on the binding of the HIV-1 gp120 V3 loop to CXCR4 (entry inhibition) (Doranz et al., 1997; Murakami et al., 1999). Our synthesized peptides contained an arginine-rich motif in their sequences and blocked early-phase infection only by the CXCR4-tropic HIV-1_{IIIB} virus. Therefore, we investigated whether the anti-HIV-1 activities of these peptides in the early phase were produced by CXCR4 antagonism using flow cytometric analysis with an anti-CXCR4 monoclonal antibody (MAb; 12G5). All the peptides, including $Rev_{34\text{-}50}$-A_4C, $Rev_{34\text{-}50}$-

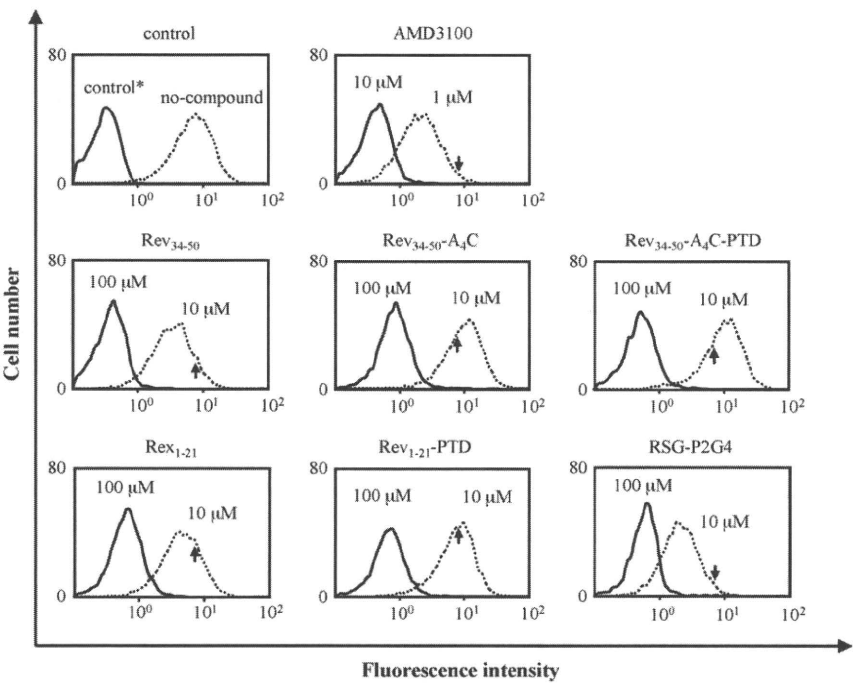

Fig. 2. Effects of the peptides on binding of a MAb against CXCR4 expressed on the MT-2 cell surface. MT-2 cells were resuspended in PBS containing 1% FCS and preincubated with the peptides at 4 °C for 30 min. PE-conjugated anti-CXCR4 MAb (12G5) was then added and incubated at 4 °C for a further 30 min. The cells were washed three times, fixed with 1% formaldehyde, and analyzed using a flow cytometer. A CXCR4 antagonist, AMD3100, was used a positive control. The results represent one of three independent experiments. (*) Fluorescence without PE-conjugated 12G5 is shown. Arrowhead indicates the mean fluorescence intensity of the no compound control.

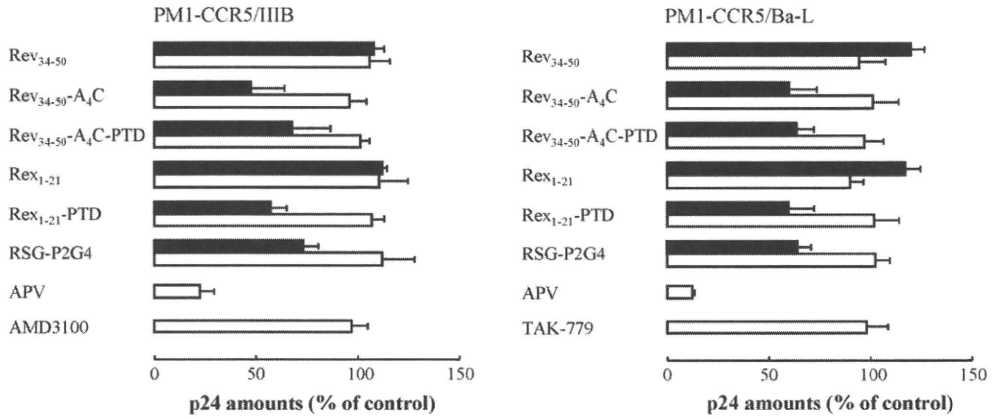

Fig. 3. Inhibitory effects of the peptides on p24 production from persistently HIV-1-infected PM1-CCR5 cells. PM1-CCR5 cells persistently infected with HIV-1_{IIIB} or HIV-1_{Ba-L} (PM1-CCR5/IIIB or PM1-CCR5/Ba-L cells, respectively) were washed and resuspended at 4×10^4 cells/ml with the peptides (black bars: 10 μM; white bars: 1 μM), APV as a positive control or AMD3100, TAK-779 or medium alone (control) as negative controls. After 48 h, the amounts of viral p24 in the culture supernatants were measured. The results are expressed as the percentages of p24 relative to that of the control. The data represent the means + SD of three independent experiments.

A_4C-PTD and Rex_{1-21}-PTD (data not shown), inhibited binding of 12G5 in a dose-dependent manner as observed for AMD3100 (Fig. 2). Although Rex_{1-21} showed only weak inhibitory activity against HIV-1_{IIIB} at 10 μM (data not shown), it blocked the binding of 12G5 sufficiently at 100 μM (Fig. 2). Relatively high concentrations of peptides were required to block binding of 12G5. It is likely that numerous functional and non-functional CXCR4 for HIV-1 infection may be expressed on the cell surface. In the CCR5 case, the antagonism observed in less than 20% of cell surface expressed CCR5 appeared to be sufficient for inhibition of HIV infection (Maeda et al., 2004), since only that to functional CCR5 as an HIV-1 receptor, including co-localization with CD4, appears to be required. However, for a flow cytometer analysis, monoclonal antibodies and small agents including peptides can recognize both functional and non-functional, therefore, high concentration seems to be needed. Actually, another peptide CXCR4 antagonist, T134 was also required high concentration to inhibit 12G5 binding in a flow cytometry (Arakaki et al., 1999). These results indicate that the arginine-rich peptides may inhibit infection by HIV-1_{IIIB} through antagonism for CXCR4.

3.3. Inhibitory effects against viral production

In addition of the CXCR4 antagonism, the inhibitory effects of the peptides in the late phase were independently evaluated using persistently HIV-1-infected PM1-CCR5 cells. AMD3100, TAK-779 and the protease inhibitor APV were used as controls. The specific CXCR4 or CCR5 antagonists AMD3100 and TAK-779, respectively, had no inhibitory effects on viral production, whereas APV (1 μM) effectively inhibited the production of viral p24 antigen from both PM1-CCR5/IIIB and PM1-CCR5/Ba-L cells (Fig. 3). Rev_{34-50}, which specifically binds to the RRE similar to intact Rev *in vitro* (Kjems et al., 1992), showed no inhibitory effects on the production of viral p24, whereas Rev_{34-50}-A_4C inhibited the production of p24 from both PM1-CCR5/IIIB and PM1-CCR5/Ba-L cells. Addition of Tat-PTD to Rev_{34-50}-A_4C, which provides cell permeability, hardly enhanced the inhibitory effect. On the other hand, although Rex_{1-21} had no effect on the production of viral p24, Rex_{1-21}-PTD inhibited the production of viral p24 from both PM1-CCR5/IIIB and PM1-CCR5/Ba-L cells. RSG-P2G4, which interacts with the RRE more tightly than Rev_{34-50} (Harada et al., 1997), also inhibited the production of p24 from both PM1-CCR5/IIIB and PM1-CCR5/Ba-L cells. However, the antiviral activities of Rev_{34-50}-A_4C, Rev_{34-50}-A_4C-PTD and Rex_{1-21}-PTD were comparable to that of RSG-P2G4. None of the peptides showed any cytotoxicity for 5 days, as evaluated by 3-(4,5-dimethylthiazol-2-yl)-2,5-diphenyltetrazolium bromide (MTT) assays (data not shown).

3.4. Infectivity of secreted HIV-1

To address whether HIV-1 secreted from the persistently infected PM-1 treated with peptides, maintains its infectivity, we examined the infectivity of HIV-1 particles in the supernatant. To avoid effect of CXCR4 antagonism by the peptides, we used HIV-1_{Ba-L} strain for the experiments. PM1-CCR5/Ba-L cells were washed 3 times and exposed to each peptide (10 μM) for 24 h. The supernatant, which contains newly produced and secreted HIV-1_{Ba-L}, was harvested and subjected to the titration with the MAGI cells and the p24 assay. $Rev_{3450A4C}$ attenuated the infectivity compared to the anticipated one by p24, while other peptides, Rev_{3450} and P2G4 showed moderately reduced infectivity (Table 2). However, both Rex-derived peptides showed little changes in actual and anticipated infectivity. These results indicate that the peptides, especially $Rev_{34-50}A_4C$, might sustain its binding to the RRE even in the virion and/or during RT reaction after the next round of the new infection, led to the reduced infectivity.

3.5. Anti-HIV-1 effects on intracellular expression of Rev peptides

The arginine-rich peptides inhibited the production of p24 in PM1-CCR5 cells persistently infected with HIV-1 (Fig. 3). Next, we evaluated the effects of intracellular expression of various Rev mutants in MT-2 cells against HIV-1 infection using MTT assays.

Table 2
Peptide effect on infectivity of HIV-1_{Ba-L}.

Compound	% of non-treated control		Infectivity/p24
	Infectivity	p24	
Rev_{34-50}	74 ± 11	119 ± 16	0.62
Rev_{34-50}-A_4C	24 ± 1	67 ± 8	0.36
Rex_{1-21}	121 ± 43	93 ± 24	1.3
Rex_{1-21}-PTD	74 ± 30	82 ± 15	0.97
RSG-P2G4	72 ± 32	92 ± 5	0.78

Infectivity and amount of p24 in the supernatant of PM1-CCR5/Ba-L cells exposed to peptides (10 μM) were determined by the MAGI assay and a commercially available p24 kit, respectively. Each value was normalized by that of simultaneously performed non-treated control as 100%. Data represent the means ± SD of three independent experiments.

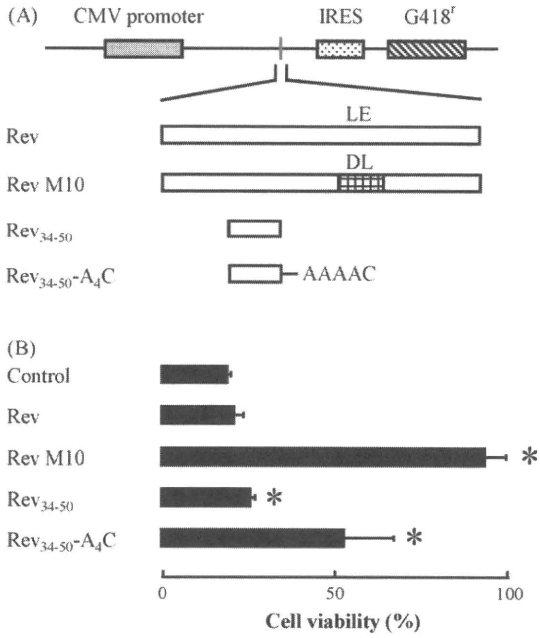

Fig. 4. Anti-HIV-1 activities of various Rev-transduced MT-2 cells. (A) Structures of the pCI-Rev-IG expression vectors encoding various Rev mutants. The fragments encoding Rev, Rev M10 ($D_{78}L_{79}$), Rev_{34-50} and Rev_{34-50}-A_4C were inserted into the upstream of IRES-$G418^r$ under the control of the CMV promoter. Amino acid substitutions at $L_{78}E_{79}$ (wild type Rev) to $D_{78}L_{79}$ (Rev dominant-negative mutant, Rev M10) diminish nuclear export of HIV mRNA (Malim and Cullen, 1991). (B) Effects of various Rev mutant transductions on HIV-1. MT-2 cells were transfected with various Rev mutant-encoding vectors and subjected to G418 selection. The Rev-transduced cells were infected with $HIV\text{-}1_{IIIB}$. On day 5 post-infection, the cell viabilities were determined by the MTT assay. The assays were performed in triplicate and the means + SD are shown. The results are representative of three independent experiments. $^*p < 0.05$, significant difference to the control by Student's *t*-test.

To obtain such MT-2 cells, the cells were transfected with various Rev expression vectors and then selected by G418. Although the expression of Rev hardly affected the cell death caused by HIV-1 infection, transduction of Rev M10, a dominant-negative mutant of Rev lacking NES activity, dramatically conferred resistance against HIV-1 infection (Fig. 4). Transduction of Rev_{34-50} moderately protected the cells. However, Rev_{34-50}-A_4C-transduced cells became more resistant to HIV-1 infection than Rev_{34-50}-transduced cells. These results for the transduced cells are consistent with those obtained for the persistently HIV-1-infected cells (Fig. 3). Therefore, the intracellular expression of Rev peptides conferred resistance against HIV-1 infection.

3.6. Subcellular localizations of Rev and Rex peptides

To elucidate the inhibitory mechanism of the arginine-rich peptides in the late phase of the replication cycle, we constructed $pRev_{peptide}$-EGFP and $pRex_{peptide}$-EGFP vectors expressing C-terminally EGFP-fused Rev and Rex peptides and examined the subcellular localizations of the EGFP-fused Rev and Rex peptides. In 293T cells, EGFP alone was equally distributed throughout the cells (Fig. 5, the 1st panel Control). In contrast, Rev and Rev M10 were mostly detected in nucleoli as previously reported (Dundr et al., 1995; Kalland et al., 1994; Stauber et al., 1995). Rev_{34-50}, Rev_{34-50}-A_4C and Rex_{1-21} were moderately detected in the cytoplasm, but dominantly accumulated in the nucleus. Similar results were observed in NP-2 cells (data not shown). These results indicate that Rev peptides exert antiviral activity in the same manner as Rev M10.

4. Discussion

4.1. Rev- and Rex-derived peptides act as dual antagonists toward CXCR4 and Rev

In the present study, we have demonstrated that arginine-rich peptides corresponding to the RRE-binding domains of HIV-1 Rev and HTLV-I Rex have dual inhibitory effects, namely CXCR4 antagonism and a dominant-negative effect for Rev function. Addition of A_4C, which stabilizes the α-helical structure (Lin et al., 2004), to Rev_{34-50} enhanced the inhibitory effects toward both CXCR4 antagonism and Rev function. It has been demonstrated that Rev_{34-50} forms an α-helical structure (Battiste et al., 1996; Tan et al., 1993) and binds to the RRE more efficiently when its α-helicity is increased (Tan et al., 1993). Short α-helical peptides (>20 amino acids) are known to have unstable helical structures and their helical structure is stabilized as their length increases (Marqusee et al., 1989). Hence, it is likely that the expected increase in α-helicity of Rev_{34-50} by the addition of A_4C resulted in enhanced CXCR4 antagonism and inhibition of p24 production at a post-transcriptional step for HIV-1 genes. The Rev peptides lacked NES activity, similar to the case of Rev M10, which is a trans-dominant repressor of Rev function (Malim et al., 1989a; Malim and Cullen, 1991). Therefore, the peptides may inhibit HIV-1 replication by competing with Rev for binding to the RRE, similar to the case of Rev M10. We observed that the Rev peptides, which contained a NLS, accumulated in the nucleoli. Expression of Rev M10 inhibited the cell death caused by HIV-1 significantly more efficiently than Rev_{34-50}-A_4C. This may be the result of Rev_{34-50}-A_4C being able to inhibit only the Rev-RRE binding step, whereas Rev M10 can inhibit multiple Rev functions

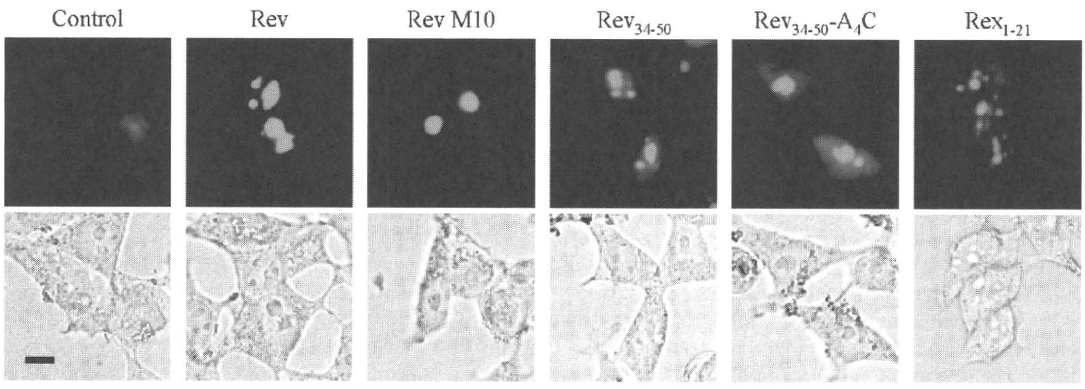

Fig. 5. Subcellular localizations of Rev and Rex peptides. 293T cells were transfected with $pRev_{peptide}$-EGFP and $pRex_{peptide}$-EGFP plasmids expressing Rev-, Rev M10-, Rev_{34-50}-, Rev_{34-50}-A_4C- and Rex_{1-21}-EGFP fusion proteins and EGFP alone as a control. After 48 h, the cells were fixed and examined using a fluorescence microscope (excitation: 488 nm). Fluorescent (upper panels) and corresponding phase-contrast (lower panels) images are shown. Scale bar: 10 μm.

by forming Rev-Rev M10 hetero-oligomers lacking NES activity (Stauber et al., 1995). However, despite the higher potency of Rev M10, its clinical applications are limited because it only differs from Rev by two amino acids. In this regard, the short peptide Rev_{34-50}-A_4C is more well suited for clinical applications. In fact, enfuvirtide (T-20), a similar 36-amino acid long peptide which inhibits HIV-1 fusion has been approved for the treatment of HIV infections and its clinical efficacy and utility has been demonstrated (Lalezari et al., 2003; Lazzarin et al., 2003).

Although addition of Tat-PTD may enhance the cell permeability of the peptides, its effects on cell permeability may be limited because the Rev and Rex peptides showed efficient cell permeability, as previously described (Futaki et al., 2001). It has been reported (Futaki et al., 2001) that peptides containing 6 and 8 arginine residues show efficient cell permeability. It is likely that addition of Tat-PTD to Rev_{34-50}-A_4C or Rex_{1-21}-A_4C hardly affected their cell permeability, as they already contained a large number of arginines. Notably, Tat-PTD does not interact with the RRE (Harada et al., 1996). On the other hand, Rex_{1-21} itself has sufficient cell permeability (Futaki et al., 2001), and addition of Tat-PTD to Rex_{1-21} enhanced its inhibitory activity likely through interactions with the CXCR4 coreceptor. Specifically, although Rex_{1-21} showed a weak antagonistic effect against CXCR4 by itself, addition of Tat-PTD to Rex_{1-21} enhanced its antagonistic effect because Tat-PTD contains an arginine-rich motif. These results indicate that the secondary structure and/or arginine content of peptides may be important for CXCR4 antagonism.

Since Rex_{1-21} accumulated in the nucleoli and Rex binds to the stem-loop III/IV/V region of the RRE, which is different from the recognition site of Rev (stem-loop IIB) (Ahmed et al., 1990; Kjems et al., 1992), Rex_{1-21}-PTD probably inhibited the production of viral p24 by interfering with an event after the Rev-stem-loop IIB interaction, possibly Rev oligomerization. It is possible that the increased size of Rex_{1-21}-PTD over Rex_{1-21} results somehow to increased steric hindrance that prevents REV oligomerization. It is also possible that the increased size of Rex_{1-21}-PTD over Rex_{1-21}- confers higher stability to the secondary structure of the peptide for binding to the RRE or competing with the Rev function in Rex_{1-21}. Binding of Rex_{1-21}-PTD to the stem-loop III/IV/V region, which is different from the binding of Rev (Ahmed et al., 1990), also inhibited p24 production, indicating that not only stem-loop IIB but also the whole RRE structure may represent potential drug targets. Moreover, it provides opportunities for combination therapies of peptides that target different domains of RRE.

RSG-P2G4, another arginine-rich peptide which permeates the cell membrane efficiently, (Harada et al., 1997), also inhibited viral p24 production. RSG-P2G4 binds to stem-loop IIB of the RRE (Harada et al., 1997), and therefore inhibited p24 production as efficiently as the Rev peptides.

4.2. Potential of Rev antagonists as chemotherapeutic agents

In the early phase of the HIV-1 replication cycle, Tat protein promotes production early proteins such as Tat, Rev and Nef. Since Tat enhances viral transcription without controlling splicing, the early proteins accumulate in the cells. One of the early proteins, Rev, inhibits splicing of the transcripts and exports them to the cytoplasm to generate late proteins including Gag, Pol, Env and progenitor genomes, resulting in suppression of Tat and Rev expression (Felber et al., 1990; Seelamgari et al., 2004). These decreases subsequently increase Tat expression, such that Tat and Rev cooperate for efficient viral gene expression with a certain balance. This cooperation plays an important role in the generation of progeny viruses, suggesting that interference with this cooperation may be sufficient for suppression of viral replication. Limited loss of Rev function without full suppression of its activity may cause an imbalance of Tat/Rev functions, resulting in dysregulation of viral expression and the formation of incomplete viruses. Therefore, only partial inhibitory effects of Rev inhibitors, rather than the full inhibition observed for reverse transcriptase and protease inhibitors, may be sufficient for effective viral suppression. In the state of Tat dominance, infected cells will keep producing disproportionate amounts of early proteins, such as Tat, Rev and Nef. Accumulation of such proteins may be detrimental to an antigen-presenting cell, as it may result in targeting by the host immune system, and elimination of infected cells. This would be a novel strategy for eliminating HIV-infected cells using peptide-based therapies.

As with all potential anti-HIV therapeutics a concern regarding Rev inhibitors is the development of resistance. However, it should be noted that in this case there would be additional constraints that are likely to affect the barrier to resistance. Specifically, introduction of mutations into the Rev coding region also influences the Tat and/or Env sequences and possibly their functions, as both proteins are simultaneously encoded with Rev. Furthermore, it is likely that successful introduction of mutations might interfere with the balance of Rev/Tat, which would also reduce viral replication and lead to possible elimination of the infected cells by the host immune system. In the case of RRE mutations, we have clearly demonstrated that the RRE and the gp41 N-heptad repeat (N-HR), one of the key helical domains for virus fusion, are simultaneously encoded and that mutations in the N-HR influenced RRE structure clearly affect the replication kinetics of the virus (Nameki et al., 2005; Ueno et al., 2009). These observations highlight a number of difficulties that HIV-1 would have to overcome in order to develop resistance against Rev inhibitors. Even if HIV-1 does acquire resistance, this may result in deteriorating replication kinetics, since it will simultaneously alter the functions of other viral proteins, such as Tat and gp41, and the RRE. Therefore, genetic barrier for resistance against Rev inhibitors is expected to be high and Rev inhibitors may be able to sustain antiviral activity during prolonged use.

5. Conclusion

We have shown that arginine-rich peptides derived from the RNA-binding domain of HIV-1 Rev can act as dual-target inhibitors that inhibit HIV-1 entry and viral production in the early and late phases of replication. Targeting Rev for chemotherapy is a promising strategy because it is entirely distinct from current drug targets. In addition, acquisition of resistance to Rev inhibitors may be limited because the Rev and RRE encoding regions simultaneously encode Tat and/or Env. Furthermore, the Rev peptides inhibit a completely different step of HIV-1 infection, the coreceptor CXCR4, and may, therefore, exert synergistic effects. Moreover, inhibiting Rev function may induce elimination of infected cells by the host immune system, suggesting that Rev peptides may represent the first inhibitors to enhance vaccine efficacy. Taken together, the dual-target Rev peptides are attractive agents and our present observations support their development as dual-target inhibitors for the prevention of HIV-1 infection.

Acknowledgments

We appreciate Dr. Masahiko Sugita for comments on the manuscript. We thank Dr. Kazuya Shimura, Miss Keiko Kajiwara and Mr. Makoto Shirakawa for technical assistance.

This work was supported by a grant from the Ministry of Education, Culture, Sports, Science, and Technology of Japan (E.K.), a grant for the Promotion of AIDS Research from the Ministry of Health, Labor and Welfare (to E.K. and M.M.) and a grant for Research for Health Sciences Focusing on Drug Innovation from the Japan Health Sciences Foundation (to E.K. and M.M.). K.S. is supported by the 21st

Century COE program of the Ministry of Education, Culture, Sports, Science and Technology.

References

Ahmed YF, Hanly SM, Malim MH, Cullen BR, Greene WC. Structure-function analyses of the HTLV-I Rex and HIV-1 Rev RNA response elements: insights into the mechanism of Rex and Rev action. Genes Dev 1990;4:1014–22.

Arakaki R, Tamamura H, Premanathan M, Kanbara K, Ramanan S, Katsura Mochizuki K, et al. T134, a small-molecule CXCR4 inhibitor, has no cross-drug resistance with AMD3100, a CXCR4 antagonist with a different structure. J Virol 1999;73:1719–23.

Baba M, Nishimura O, Kanzaki N, Okamoto M, Sawada H, Iizawa Y, et al. A small-molecule, nonpeptide CCR5 antagonist with highly potent and selective anti-HIV-1 activity. Proc Natl Acad Sci U S A 1999;96:5698–703.

Battiste JL, Mao H, Rao NS, Tan R, Muhandiram DR, Kay LE, et al. Alpha helix-RNA major groove recognition in an HIV-1 rev peptide-RRE RNA complex. Science 1996;273:1547–51.

Bogerd HP, Huckaby GL, Ahmed YF, Hanly SM, Greene WC. The type I human T-cell leukemia virus (HTLV-I) Rex trans-activator binds directly to the HTLV-I Rex and the type 1 human immunodeficiency virus Rev RNA response elements. Proc Natl Acad Sci U S A 1991;88:5704–8.

Charpentier B, Stutz F, Rosbash M. A dynamic in vivo view of the HIV-I Rev-RRE interaction. J Mol Biol 1997;266:950–62.

Daugherty MD, D'Orso I, Frankel AD. A solution to limited genomic capacity: using adaptable binding surfaces to assemble the functional HIV Rev oligomer on RNA. Mol Cell 2008;31:824–34.

Dayton ET, Powell DM, Dayton AI. Functional analysis of CAR, the target sequence for the Rev protein of HIV-1. Science 1989;246:1625–9.

Donzella GA, Schols D, Lin SW, Este JA, Nagashima KA, Maddon PJ, et al. AMD3100, a small molecule inhibitor of HIV-1 entry via the CXCR4 co-receptor. Nat Med 1998;4:72–7.

Doranz BJ, Grovit-Ferbas K, Sharron MP, Mao SH, Goetz MB, Daar ES, et al. A small-molecule inhibitor directed against the chemokine receptor CXCR4 prevents its use as an HIV-1 coreceptor. J Exp Med 1997;186:1395–400.

Dundr M, Leno GH, Hammarskjold ML, Rekosh D, Helga-Maria C, Olson MO. The roles of nucleolar structure and function in the subcellular location of the HIV-1 Rev protein. J Cell Sci 1995;108(Pt 8):2811–23.

Este JA, Telenti A. HIV entry inhibitors. Lancet 2007;370:81–8.

Felber BK, Drysdale CM, Pavlakis GN. Feedback regulation of human immunodeficiency virus type 1 expression by the Rev protein. J Virol 1990;64:3734–41.

Felber BK, Hadzopoulou-Cladaras M, Cladaras C, Copeland T, Pavlakis GN. rev protein of human immunodeficiency virus type 1 affects the stability and transport of the viral mRNA. Proc Natl Acad Sci U S A 1989;86:1495–9.

Fischer U, Huber J, Boelens WC, Mattaj IW, Luhrmann R. The HIV-1 Rev activation domain is a nuclear export signal that accesses an export pathway used by specific cellular RNAs. Cell 1995;82:475–83.

Futaki S, Ishikawa T, Niwa M, Kitagawa K, Yagami T. Embodying a stable alpha-helical protein structure through efficient chemical ligation via thioether formation. Bioorg Med Chem 1997;5:1883–91.

Futaki S, Suzuki T, Ohashi W, Yagami T, Tanaka S, Ueda K, et al. Arginine-rich peptides. An abundant source of membrane-permeable peptides having potential as carriers for intracellular protein delivery. J Biol Chem 2001;276:5836–40.

Hammes SR, Greene WC. Multiple arginine residues within the basic domain of HTLV-I Rex are required for specific RNA binding and function. Virology 1993;193:41–9.

Harada K, Martin SS, Frankel AD. Selection of RNA-binding peptides in vivo. Nature 1996;380:175–9.

Harada K, Martin SS, Tan R, Frankel AD. Molding a peptide into an RNA site by in vivo peptide evolution. Proc Natl Acad Sci U S A 1997;94:11887–92.

Jain C, Belasco JG. Structural model for the cooperative assembly of HIV-1 Rev multimers on the RRE as deduced from analysis of assembly-defective mutants. Mol Cell 2001;7:603–14.

Jiang F, Gorin A, Hu W, Majumdar A, Baskerville S, Xu W, et al. Anchoring an extended HTLV-1 Rex peptide within an RNA major groove containing junctional base triples. Structure 1999;7:1461–72.

Kalland KH, Szilvay AM, Langhoff E, Haukenes G. Subcellular distribution of human immunodeficiency virus type 1 Rev and colocalization of Rev with RNA splicing factors in a speckled pattern in the nucleoplasm. J Virol 1994;68:1475–85.

Kjems J, Calnan BJ, Frankel AD, Sharp PA. Specific binding of a basic peptide from HIV-1 Rev. EMBO J 1992;11:1119–29.

Kodama EI, Kohgo S, Kitano K, Machida H, Gatanaga H, Shigeta S, et al. 4'-Ethynyl nucleoside analogs: potent inhibitors of multidrug-resistant human immunodeficiency virus variants in vitro. Antimicrob Agents Chemother 2001;45:1539–46.

Lalezari JP, Henry K, O'Hearn M, Montaner JS, Piliero PJ, Trottier B, et al. Enfuvirtide, an HIV-1 fusion inhibitor, for drug-resistant HIV infection in North and South America. N Engl J Med 2003;348:2175–85.

Lazzarin A, Clotet B, Cooper D, Reynes J, Arasteh K, Nelson M, et al. Efficacy of enfuvirtide in patients infected with drug-resistant HIV-1 in Europe and Australia. N Engl J Med 2003;348:2186–95.

Lin JC, Barua B, Andersen NH. The helical alanine controversy: an (Ala)6 insertion dramatically increases helicity. J Am Chem Soc 2004;126:13679–84.

Maeda K, Nakata H, Koh Y, Miyakawa T, Ogata H, Takaoka Y, et al. Spirodiketopiperazine-based CCR5 inhibitor which preserves CC-chemokine/CCR5 interactions and exerts potent activity against R5 human immunodeficiency virus type 1 in vitro. J Virol 2004;78:8654–62.

Malim MH, Bohnlein S, Hauber J, Cullen BR. Functional dissection of the HIV-1 Rev trans-activator—derivation of a trans-dominant repressor of Rev function. Cell 1989a;58:205–14.

Malim MH, Cullen BR. HIV-1 structural gene expression requires the binding of multiple Rev monomers to the viral RRE: implications for HIV-1 latency. Cell 1991;65:241–8.

Malim MH, Hauber J, Le SY, Maizel JV, Cullen BR. The HIV-1 rev trans-activator acts through a structured target sequence to activate nuclear export of unspliced viral mRNA. Nature 1989b;338:254–7.

Mann DA, Mikaelian I, Zemmel RW, Green SM, Lowe AD, Kimura T, et al. A molecular rheostat. Co-operative rev binding to stem I of the rev-response element modulates human immunodeficiency virus type-1 late gene expression. J Mol Biol 1994;241:193–207.

Marqusee S, Robbins VH, Baldwin RL. Unusually stable helix formation in short alanine-based peptides. Proc Natl Acad Sci U S A 1989;86:5286–90.

Murakami T, Zhang TY, Koyanagi Y, Tanaka Y, Kim J, Suzuki Y, et al. Inhibitory mechanism of the CXCR4 antagonist T22 against human immunodeficiency virus type 1 infection. J Virol 1999;73:7489–96.

Nagahara H, Vocero-Akbani AM, Snyder EL, Ho A, Latham DG, Lissy NA, et al. Transduction of full-length TAT fusion proteins into mammalian cells: TAT-p27Kip1 induces cell migration. Nat Med 1998;4:1449–52.

Nameki D, Kodama E, Ikeuchi M, Mabuchi N, Otaka A, Tamamura H, et al. Mutations conferring resistance to human immunodeficiency virus type 1 fusion inhibitors are restricted by gp41 and Rev-responsive element functions. J Virol 2005;79:764–70.

Olsen HS, Cochrane AW, Dillon PJ, Nalin CM, Rosen CA. Interaction of the human immunodeficiency virus type 1 Rev protein with a structured region in env mRNA is dependent on multimer formation mediated through a basic stretch of amino acids. Genes Dev 1990;4:1357–64.

Rimsky L, Hauber J, Dukovich M, Malim MH, Langlois A, Cullen BR, et al. Functional replacement of the HIV-1 rev protein by the HTLV-1 rex protein. Nature 1988;335:738–40.

Seelamgari A, Maddukuri A, Berro R, de la Fuente C, Kehn K, Deng L, et al. Role of viral regulatory and accessory proteins in HIV-1 replication. Front Biosci 2004;9:2388–413.

Siomi H, Shida H, Nam SH, Nosaka T, Maki M, Hatanaka M. Sequence requirements for nucleolar localization of human T cell leukemia virus type I pX protein, which regulates viral RNA processing. Cell 1988;55:197–209.

Stauber R, Gaitanaris GA, Pavlakis GN. Analysis of trafficking of Rev and transdominant Rev proteins in living cells using green fluorescent protein fusions: transdominant Rev blocks the export of Rev from the nucleus to the cytoplasm. Virology 1995;213:439–49.

Szilvay AM, Brokstad KA, Kopperud R, Haukenes G, Kalland KH. Nuclear export of the human immunodeficiency virus type 1 nucleocytoplasmic shuttle protein Rev is mediated by its activation domain and is blocked by transdominant negative mutants. J Virol 1995;69:3315–23.

Tan R, Chen L, Buettner JA, Hudson D, Frankel AD. RNA recognition by an isolated alpha helix. Cell 1993;73:1031–40.

Uchida H, Maeda Y, Mitsuya H. HIV-1 protease does not play a critical role in the early stages of HIV-1 infection. Antiviral Res 1997;36:107–13.

Ueno M, Kodama EN, Shimura K, Sakurai Y, Kajiwara K, Sakagami S, Oishi S, Fujii N, Matsuoka M. Synonymous mutations in stem-loop III of Rev responsive elements enhance HIV-1 replication impaired by primary mutations for resistance to enfuvirtide. Antiviral Res 2009;82:67–72.

Vodicka MA, Goh WC, Wu LI, Rogel ME, Bartz SR, Schweickart VL, Raport CJ, Emerman M. Indicator cell lines for detection of primary strains of human and simian immunodeficiency viruses. Virology 1997;233:193–8.

Zapp ML, Hope TJ, Parslow TG, Green MR. Oligomerization and RNA binding domains of the type 1 human immunodeficiency virus Rev protein: a dual function for an arginine-rich binding motif. Proc Natl Acad Sci U S A 1991;88:7734–8.

CONCISE ARTICLE www.rsc.org/medchemcomm | MedChemComm

Affinity selection and sequence-activity relationships of HIV-1 membrane fusion inhibitors directed at the drug-resistant variants†

Shinya Oishi,*[a] Kentaro Watanabe,[a] Saori Ito,[a] Michinori Tanaka,[a] Hiroki Nishikawa,[a] Hiroaki Ohno,[a] Kazuki Shimane,[b] Kazuki Izumi,[b] Yasuko Sakagami,[b] Eiichi N. Kodama,‡[b] Masao Matsuoka,[b] Akira Asai[c] and Nobutaka Fujii*[a]

Received 29th June 2010, Accepted 22nd July 2010
DOI: 10.1039/c0md00091d

Enfuvirtide is the first approved membrane fusion inhibitor against HIV-1. Although this drug is effective against multi-drug resistant strains, the emergence of enfuvirtide-resistant strains has been reported in patients who have received an enfuvirtide-containing regimen. Based on the high affinity of synthetic HIV-1 gp41 C-terminal heptad repeat (C-HR) peptides to the counterpart trimeric N-terminal heptad repeat (N-HR) coiled-coil structure, a novel screening approach has been established to facilitate the identification of potent fusion inhibitors against wild-type and enfuvirtide-resistant HIV-1. In this process, affinity selection using histidine-tagged N-HR peptides with the sequences derived from wild-type and resistant strains efficiently captured potent inhibitory peptides from a pool of highly water-soluble C-HR peptides with α-helix-inducible motifs. A highly potent peptide was found from a single amino acid substitution observed in an enfuvirtide-resistant variant as well as peptides with unprecedented modifications at the mutated site.

Introduction

Several inhibitors that block viral attachment and the fusion process have been approved for the treatment of human immunodeficiency virus (HIV) in the past decade. The first fusion inhibitor, enfuvirtide (T-20), binds to the N-terminal heptad repeat (N-HR) of the HIV-1 envelop glycoprotein gp41,[1] and prevents the formation of a fusogenic antiparallel coiled-coil structure (known as the six-helical bundle) between N-HR and the C-terminal heptad repeat (C-HR) (Fig. 1a).[2] Enfuvirtide is effective even against the clinical strains that are resistant to multiple drug classes such as reverse transcriptase inhibitors and protease inhibitors used in highly active antiretroviral therapy (HAART). However, the emergence of enfuvirtide-resistant strains has been reported in patients receiving long-term enfuvirtide treatment.[3,4]

The primary evolution of enfuvirtide resistance occurs on gp41 N-HR, which attenuates the binding affinity with enfuvirtide, resulting in decreased drug susceptibility.[3–5] The major primary mutations are V38A and N43D in the Leu33–Leu45 region of N-HR. These mutations subsequently lead to a secondary mutation appearing in C-HR, which can compensate the binding affinity between viral N-HR and C-HR for efficient gp41 folding.[6] For example, N126K and S138A mutations have been reported to enhance the resistance induced by enfuvirtide and another inhibitory C-HR peptide, C34. These complementary mutations, which occur at the face-to-face positions of N-HR and C-HR verified by crystallographic studies,[7–9] can restore the critical step required for viral infection into the target cells and eliminate the inhibitory effect of exogenous enfuvirtide.

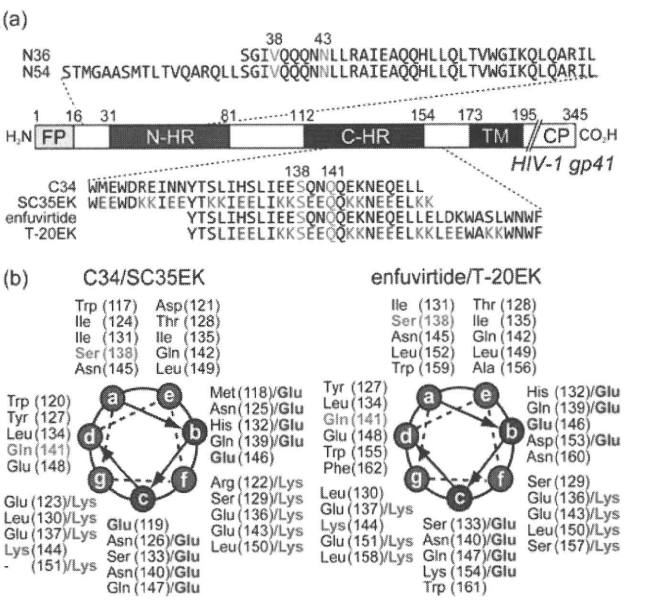

Fig. 1 HIV-1 envelope protein gp41 and the amino acid sequences. (a) Schematic representation of HIV-1 gp41. FP: fusion peptide; TM: transmembrane domain; CP: cytoplasmic tail. (b) Helical-wheel representation of C34/SC35EK and enfuvirtide/T-20EK.

[a]*Graduate School of Pharmaceutical Sciences, Kyoto University, Sakyo-ku, Kyoto 606-8501, Japan. E-mail: soishi@pharm.kyoto-u.ac.jp; nfujii@pharm.kyoto-u.ac.jp; Fax: +81-75-753-4570; Tel: +81-75-753-4551*

[b]*Laboratory of Virus Control, Institute for Virus Research, Kyoto University, Sakyo-ku, Kyoto 606-8507, Japan*

[c]*Graduate School of Pharmaceutical Sciences, University of Shizuoka, Suruga-ku, Shizuoka 422-8526, Japan*

† Electronic supplementary information (ESI) available: Additional experimental procedures, measurement of CD spectra, bioassays, and MS data. See DOI: 10.1039/c0md00091d

‡ Present address: Division of Emerging Infectious Diseases, Tohoku University School of Medicine, Sendai 980-8575, Japan

Recently, several novel fusion inhibitors such as tifuvirtide (T-1249)[10] and sifuvirtide,[11] which are effective against these enfuvirtide-resistant viruses, have been reported. We have also demonstrated a novel tailored design of fusion inhibitors based on the enfuvirtide-resistant mutation to preempt this escape strategy of HIV-1.[12] Enfuvirtide analogues carrying a substitution corresponding to the secondary mutation were found to exert potent anti-HIV activity against wild-type and enfuvirtide-resistant strains with the primary mutations. Of interest, during this observation, we found that enfuvirtide analogues with other substitutions were also effective against these strains. Alternatively, modification of a single residue in C-HR such as Q141L, which is involved in the increased syncytium-forming ability of the mutant virus,[13] led to an increase in the anti-HIV potency of inhibitor C34.[14] These observations implied that the C-HR sequence with substitutions, which were not spontaneously elaborated by single nucleotide mutations from wild-type HIV-1, could represent potent fusion inhibitors. Encouraged by these results, the optimization of interactive residues of fusion inhibitors against wild-type and enfuvirtide-resistant viruses was undertaken.

Affinity selection-mass spectrometry (AS-MS) is a promising methodology for compound screening, in which target molecule-bound components are captured from a pool of candidates and are identified by mass spectrometry. The successful applications of this technique are exemplified by the identification of kinase inhibitors[15] and antifungal natural products.[16] This simple selection process by virtue of the binding affinity can be a facile alternative to functional bioassays, although the functions and mechanisms of captured compounds for bioactivity cannot be determined. For medicinal chemistry of HIV fusion inhibitors, this approach should be suitable in the optimization of inhibitory C-HR peptides such as T-20EK[17] and SC35EK.[18] Taking advantage of the trimeric N-HR coiled-coil as a target molecule, a mixture of C-HR peptides with a single amino acid substitution can be screened without using recombinant or clinical HIV strains.[19,20] We envisioned that the competitive binding of C-HR components would capture relatively more potent anti-HIV peptides with higher affinity towards N-HR. Herein we report on the affinity-based screening technology and sequence-activity relationships for amino acid optimization in HIV-1 fusion inhibitors directed against enfuvirtide-resistant HIV strains.

Results and discussion

T-20EK and SC35EK are characterized by repeated X-EE-XX-KK motifs that stabilize the bioactive α-helix structure of enfuvirtide and C34, respectively (Fig. 1a). Potential electrostatic interactions between glutamic acid (Glu) and lysine (Lys) residues at i and $i + 4$ positions, respectively, are distinct from the traditional stabilization with stapled covalent linkages.[21,22] Consistent substitution of the residues located on the non-interactive surface of the C-HR α-helix with Glu or Lys achieved an enhancement in affinity toward the N-HR sequence and anti-HIV activity. This process disclosed the indispensable residues in C-HR for direct interaction with viral N-HR (Fig. 1b).[23] Additionally, in contrast to native sequences of C-HR peptides that are highly hydrophobic, substitution with charged amino acids markedly improved the aqueous solubility of the peptides. This design allowed us to prepare a homogeneous mixture of the SC35EK derivatives and T-20EK derivatives at high concentrations.

Initially, C-HR peptide libraries with a variety of canonical amino acid substitutions at the positions to be optimized (Ser138 and Gln141) were prepared by a split-pool method. After the construction of the C-terminal sequence using a standard Fmoc-based solid-phase peptide synthesis approach, the resin was split into fractions at position 138 or 141, where proteinogenic amino acids except for cysteine were coupled in parallel. The 19 fractions were combined again and the N-terminal sequence was constructed in one portion. All the protected peptide resins were treated with a cocktail of deprotection reagents, and the crude peptides were purified by reversed-phase HPLC to afford the expected peptides.

Separately, in order to rationalize the selection process by affinity-based technology and to investigate the sequence-activity relationship, all C-HR peptides with a single substitution were prepared in parallel and were evaluated for the biological and physicochemical properties individually. The counterpart N-HR peptides of the wild-type and enfuvirtide-resistant variants (V38A and N43D) were also prepared. For affinity selection, the histidine tag (His_6) sequence of the N-HR peptides was attached on the N-terminus *via* an aminocaproic acid-glycine dipeptide linker. This linker was incorporated to avoid the possible disruption of N-HR and C-HR interaction by positively charged His_6-tag. Anti-HIV activities of all the C-HR peptides against laboratory wild-type HIV-1_{NL4-3} or the variants with enfuvirtide-resistant mutations were evaluated using the MAGI assay. Thermal stabilities of the potential six-helical bundles consisting of N-HR and C-HR peptides were evaluated by measuring the melting temperature (T_m) using the molar ellipticity value at 222 nm in circular dichroic (CD) spectra of N36/SC35EK or N54/T-20EK mixture (Figure S1, ESI†).

The AS-MS protocol was optimized using SC35EK derivatives (Table 1). A pool of $SC35EK_{S138X}$ was incubated with a wild-type N-HR peptide, N36 (10 μM) with an N-terminal His_6-tag, in HEPES buffer (pH 7.4). The potential six-helical bundles of N36–$SC35EK_{S138X}$ were captured by Ni-NTA agarose resin and were subsequently eluted with 50% AcOH (Fig. 2a). The captured components were separated and characterized by LC-MS analysis, except that the peptides with Leu and Ile were observed as overlapping peaks of the same mass-to-charge ratio (Fig. 2b). The recovery rate in affinity selection for relative binding ability to N36 was calculated from the detected signal of $[M + 3H]^{3+}$ and $[M + 4H]^{4+}$ ions of each C-HR peptide by the LC-MS analysis of captured peptides. Under the high concentration conditions (10 μM each of $SC35EK_{S138X}$), several potent peptides including a resistant variant-derived S138A peptide were captured in high recovery rates, while slightly less potent peptides such as $SC35EK_{S138F}$ and $SC35EK_{S138Y}$ were not detected. In contrast, when the total concentration of the mixture was nearly equal to the N36 concentration (0.6 μM each of $SC35EK_{S138X}$), there was no discernible difference in the recovery rates of each peptide. The compound with the least potent anti-HIV activity in the series, $SC35EK_{S138R}$, was recovered under this equimolar concentration conditions. This recovery suggested that the method is not effective under lower concentration conditions of C-HR peptides. A condition using

Table 1 Optimization of the affinity selection protocol

	Recovery (%)[a]					
	Concentration of $SC35EK_{S138X}$/μM					
X	10	6	1	0.6	EC_{50}/nM[b]	T_m/°C[c]
Ser	22.8	19.2	11.5	5.8	1.0 ± 0.14	81.6
Ala	30.7	22.5	11.5	5.3	1.2 ± 0.12	86.4
Asp	0.7	0.0	0.0	4.3	15 ± 3.3	59.7
Glu	1.3	1.0	1.8	5.1	15 ± 0.69	66.2
Phe	0.7	0.6	4.0	6.3	1.5 ± 0.10	72.9
Gly	13.8	14.4	11.6	5.9	1.9 ± 0.26	79.1
His	0.9	0.6	2.4	5.7	1.9 ± 0.57	62.9
Ile	4.7[d]	7.6[d]	11.3[d]	6.9[d]	1.3 ± 0.54	84.6
Lys	0.2	0.1	0.0	3.6	8.2 ± 1.7	53.5
Leu	4.7[d]	7.6[d]	11.3[d]	6.9[d]	0.93 ± 0.16	83.2
Met	8.9	13.3	12.5	6.8	0.68 ± 0.06	84.1
Asn	1.1	0.5	4.3	6.4	2.2 ± 0.47	69.0
Pro	0.4	0.2	0.1	4.5	35 ± 9.2	56.1
Gln	0.9	0.5	2.1	6.1	2.4 ± 0.79	65.9
Arg	0.3	0.1	0.0	2.5	280 ± 47	52.3
Thr	9.0	12.8	11.7	5.7	1.8 ± 0.27	79.7
Val	2.8	6.0	12.1	7.0	1.9 ± 0.64	79.9
Trp	0.5	0.3	0.9	6.2	3.1 ± 0.52	66.4
Tyr	0.5	0.4	2.3	5.9	1.9 ± 0.71	68.0

[a] The recovery rate was determined from the relative detected signals of $[M + 3H]^{3+}$ and $[M + 4H]^{4+}$ ions by LC-MS analysis. [b] EC_{50} was determined as the concentration that blocked $HIV\text{-}1_{NL4\text{-}3}$ replication by 50% in the MAGI assay. To improve the replication kinetics, the D36G mutation, observed in the majority of HIV-1 strains, was introduced into the NL4-3 background used in this study. [c] T_m values were defined by the midpoint of the thermal unfolding transition state measured by monitoring the molar ellipticity at 222 nm of N36/$SC35EK_{S138X}$ mixture. [d] Combined yield of 138I and 138L derivatives.

1 μM each of $SC35EK_{S138X}$ (total 19 μM of the mixture) for affinity selection was selected for further experiments, in which the recovery rate was found to positively correlate with the stability of the six-helical bundle (Fig. 3a). Although an ideal linear correlation was not observed between the logarithmic EC_{50} of anti-HIV activity and the recovery rate (Fig. 3b), the peptides, which were captured in relatively high yields by affinity selection, exhibited highly potent anti-HIV activity.

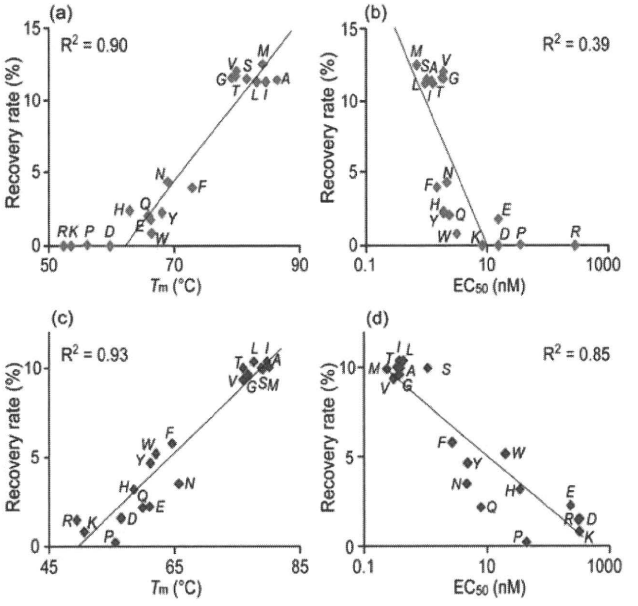

Fig. 3 Correlation between the recovery rate and the thermal stability, or the anti-HIV activity. (a, b) $SC35EK_{S138X}$; (c, d) $T\text{-}20EK_{S138X}$. R^2 values for the correlation of $SC35EK_{S138X}$ data were calculated without using the data points of S138R/K/P/D mutants ($n = 15$).

The optimized condition was applied for the selection of $T\text{-}20EK_{S138X}$ derivatives (Table 2). The anti-HIV activity of $T\text{-}20EK_{S138X}$ was found to be dependent on the amino acid type at position 138. Substitution with aliphatic side-chain amino acids such as Ala, Ile, Leu, Met and Val, displayed highly potent anti-HIV activity, although significant stabilization of the N54–$T\text{-}20EK_{S138X}$ complexes was not observed. Gly- and Thr-substitutions were also observed to increase potency. In contrast, hydrophilic, charged and aromatic amino acid substitutions at position 138 reduced binding with N54. In our previous study, it was demonstrated that higher affinity with the N-HR sequence and more potent anti-HIV activity of $C34_{S138A}$ and $T\text{-}20_{S138A}$ were due to the dominant contribution of larger desolvation free energy of the hydrophobic side-chain.[8] The structure–activity

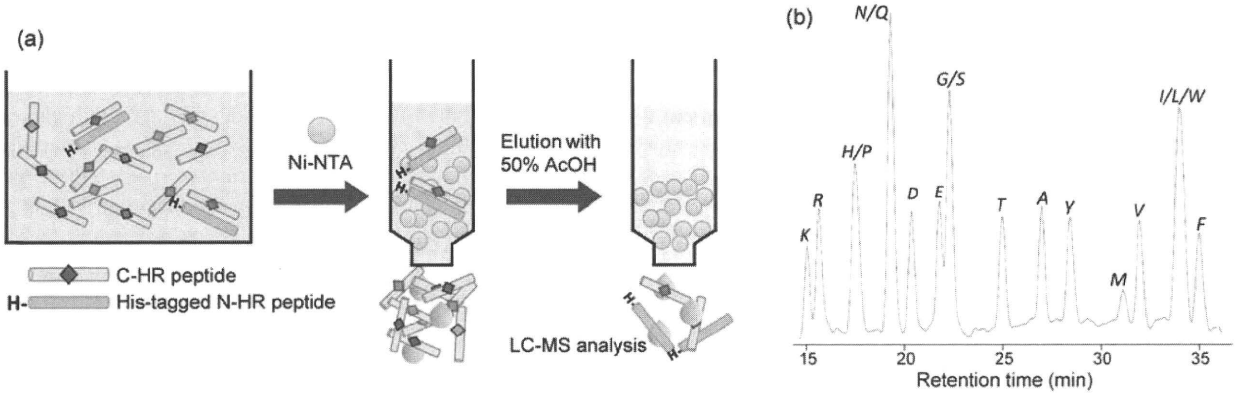

Fig. 2 Affinity selection of the HIV-1 fusion inhibitors. (a) Protocol outlining the affinity selection of C-HR peptides using the histidine-tagged N-HR peptide. (b) HPLC profile of a pool of SC35EK derivatives with a single amino acid substitution at position 138 [Cosmosil 5C18 AR-II column; linear 30–40% MeCN gradient over 40 min; flow rate, 1 $cm^3\ min^{-1}$; detection at 220 nm].

Table 2 Recovery rate in affinity selection and anti-HIV activity of T-20EK$_{S138X}$, and the thermal stability of the N54–T-20EK$_{S138X}$ complex

X	Recovery (%)[a]	EC_{50}/nM[b]	T_m/°C[c]	X	Recovery (%)[a]	EC_{50}/nM[b]	T_m/°C[c]
Ser	10.0	1.1 ± 0.2	78.8				
Ala	10.0	0.3 ± 0.1	80.1	Met	9.9	0.2 ± 0.1	79.0
Asp	1.5	330 ± 96	56.5	Asn	3.5	4.8 ± 1.6	65.7
Glu	2.2	230 ± 31	61.0	Pro	0.2	44 ± 8	55.5
Phe	5.8	2.8 ± 0.2	64.6	Gln	2.2	7.9 ± 3.4	60.0
Gly	9.6	0.4 ± 0.2	76.7	Arg	1.5	320 ± 88	49.4
His	3.2	35 ± 10	58.5	Thr	10.0	0.4 ± 0.2	75.9
Ile	10.4[d]	0.4 ± 0.1	79.7	Val	9.4	0.3 ± 0.1	76.0
Lys	0.8	330 ± 67	50.6	Trp	5.2	20 ± 9	62.0
Leu	10.4[d]	0.4 ± 0.3	77.6	Tyr	4.7	5.0 ± 1.5	61.1

[a] The recovery rate was determined from the relative detected signals of $[M + 3H]^{3+}$ and $[M + 4H]^{4+}$ ions by LC-MS analysis. [b] EC_{50} was determined as the concentration that blocked HIV-1_{NL4-3} replication by 50% in the MAGI assay. To improve the replication kinetics, the D36G mutation, observed in the majority of HIV-1 strains, was introduced into the NL4-3 background used in this study. [c] T_m values were defined by the midpoint of the thermal unfolding transition state measured by monitoring the molar ellipticity at 222 nm of N54/T-20EK$_{S138X}$ mixture. [d] Combined yield of 138I and 138L derivatives.

Table 3 Peptide recovery in affinity selection, anti-HIV activity and thermal stability of the six-helix bundles of C-HR peptides against enfuvirtide-resistant variants

	SC35EK$_{S138X}$			T-20EK$_{S138X}$		
X	Recovery (%)[a]	EC_{50}/nM[b]	T_m/°C[c]	Recovery (%)[a]	EC_{50}/nM[b]	T_m/°C[c]
HIV$_{V38A}$						
Ser	11.8	1.1 ± 0.3	72.6	9.3	3.4 ± 1.4	60.0
Ala	11.4	0.7 ± 0.2	76.1	10.0	2.2 ± 0.8	64.6
Leu	10.3[d]	0.8 ± 0.1	75.0	10.1[d]	3.4 ± 1.6	57.5
Pro	0.4	340 ± 61	56.3	0.0	>1000	49.7
Thr	10.8	0.8 ± 0.1	70.4	8.1	28 ± 12	57.8
Trp	1.0	22 ± 5.6	64.6	7.7	>1000	53.2
HIV$_{N43D}$						
Ser	10.9	0.3 ± 0.1	69.9	7.4	2.0 ± 0.4	65.3
Ala	12.9	0.2 ± 0.1	74.4	10.2	0.3 ± 0.1	71.9
Leu	12.9[d]	0.2 ± 0.1	80.0	10.8[d]	0.2 ± 0.1	74.0
Pro	0.3	130 ± 52	55.6	0.3	430 ± 160	55.0
Thr	9.4	0.3 ± 0.1	67.5	6.1	3.7 ± 0.1	62.4
Trp	2.4	2.7 ± 0.6	66.0	7.6	220 ±17	61.4

[a] The recovery rate was determined from the relative detected signals of $[M + 3H]^{3+}$ and $[M + 4H]^{4+}$ ions by LC-MS analysis. [b] EC_{50} was determined as the concentration that blocked HIV-1_{NL4-3} replication by 50% in the MAGI assay. To improve the replication kinetics, the D36G mutation, observed in the majority of HIV-1 strains, was introduced into the NL4-3 background used in this study. [c] T_m values were defined by the midpoint of the thermal unfolding transition state measured by monitoring the molar ellipticity at 222 nm of N36$_{V38A}$/SC35EK$_{S138X}$, N36$_{N43D}$/SC35EK$_{S138X}$, N54$_{V38A}$/T-20EK$_{S138X}$ or N54$_{N43D}$/T-20EK$_{S138X}$ mixture. [d] Combined yield of 138I and 138L derivatives.

relationship of T-20EK$_{S138X}$ can be partially rationalized by the similar hydrophobic/hydrophilic properties of the side-chain. The recovery rates of T-20EK$_{S138X}$ in affinity selection showed good correlations with both anti-HIV activity and with thermal stability of the complexes (Fig. 3c and 3d). The peptides captured with more than 9% recovery yields exhibited sub-nanomolar potency along with T_m values >75 °C.

The anti-HIV activities of the series of peptides against recombinant viruses with either the enfuvirtide-resistant V38A or N43D mutation in N-HR were evaluated. The results of representative C-HR peptides, which were obtained by a single nucleotide mutation of HIV-1_{NL4-3}, are shown in Table 3 and Figure S2.† From Ser138 encoded by the TCG codon in wild-type NL4-3, Ala (GCG), Pro (CCG), Thr (ACG), Leu (TTG) and Trp (TGG) are possible mutations; the other mutations are silent (TCA, TCT, TCC) or a stop codon (TAG). The S138A substitution in both SC35EK and T-20EK enhanced the thermal stability of the N-HR/C-HR complex, indicating that this is a favorable mutation in terms of gp41 folding of the resistant virus.[3,4] These peptides by mutant-directed design restored and enhanced the anti-HIV activity against enfuvirtide-resistant variants. The S138L peptide was also effective against both V38A and N43D strains; however, no emergence of a clinical variant having this mutation has been reported. Of interest, resistant viruses are unlikely to necessarily use the best C-HR substitution to complement the gp41 folding, presumably due to the low replication kinetics. These results indicate that the mutations observed in clinical variants can direct the position to be optimized for inhibitor design but not the most appropriate amino acids. In practice, several other substitutions by Ile and Met, which are irrelevant to single nucleotide mutations from the wild-type, also provided potent anti-HIV activity against the resistant strains (Table S4, ESI†). In contrast, substitution with Pro or Trp for both peptides significantly decreased the activity,

Table 4 Peptide recovery in affinity selection, anti-HIV activity and thermal stability of the six-helix bundles of $SC35EK_{Q141X}$ and $T\text{-}20EK_{Q141X}$ derivatives

	$SC35EK_{Q141X}$			$T\text{-}20EK_{Q141X}$		
X	Recovery (%)[a]	EC_{50}/nM[b]	T_m/°C[c]	Recovery (%)[a]	EC_{50}/nM[b]	T_m/°C[c]
Gln	10.1	2.6 ± 0.3	81.6	8.2[e]	1.5 ± 0.6	78.8
Ala	6.6	1.6 ± 0.6	76.1	5.6	2.7 ± 0.3	70.4
Asp	4.5	2.9 ± 0.1	75.1	8.2	3.5 ± 0.7	71.4
Glu	4.3	2.4 ± 0.4	76.2	8.2[e]	3.8 ± 0.8	71.8
Phe	5.7	2.6 ± 0.4	76.7	5.3	2.6 ± 0.9	64.0
Gly	3.8	2.3 ± 0.7	71.0	3.4	3.0 ± 0.6	66.2
His	4.3	2.0 ± 0.5	72.6	3.7	3.0 ± 0.6	68.4
Ile	8.2[d]	2.9 ± 0.4	79.7	10.4[d]	0.8 ± 0.3	74.0
Lys	4.8	2.7 ± 0.5	69.2	4.8	3.8 ± 0.3	65.3
Leu	8.2[d]	2.7 ± 0.9	83.8	10.4[d]	0.5 ± 0.2	77.4
Met	6.0	2.0 ± 0.3	80.2	9.2	0.9 ± 0.1	74.6
Asn	4.0	2.5 ± 0.5	73.4	4.4	3.6 ± 0.7	69.0
Pro	0.0	58 ± 16	60.2	0.3	>1000	52.0
Arg	7.6	2.5 ± 0.1	71.5	7.2	1.5 ± 0.3	68.9
Ser	4.0	2.5 ± 0.7	72.4	3.2	4.6 ± 1.4	66.7
Thr	7.3	3.2 ± 0.6	76.7	6.9	2.1 ± 0.5	71.6
Val	6.2	2.2 ± 0.6	77.7	6.1	2.9 ± 0.2	70.5
Trp	7.1	1.7 ± 0.2	77.1	8.1	2.5 ± 0.1	68.8
Tyr	5.5	2.2 ± 0.6	76.3	4.9	2.3 ± 0.9	67.7

[a] The recovery rate was determined from the relative detected signals of $[M + 3H]^{3+}$ and $[M + 4H]^{3+}$ ions by LC-MS analysis. [b] EC_{50} was determined as the concentration that blocked $HIV\text{-}1_{NL4\text{-}3}$ replication by 50% in the MAGI assay. To improve the replication kinetics, the D36G mutation, observed in the majority of HIV-1 strains, was introduced into the NL4-3 background used in this study. [c] T_m values were defined by the midpoint of the thermal unfolding transition state measured by monitoring the molar ellipticity at 222 nm of $N36/SC35EK_{Q141}$ or $N54/T\text{-}20EK_{Q141}$ mixture. [d] Combined yield of 141I and 141L derivatives. [e] Combined yield of 141E and 141Q derivatives.

which is consistent with the results against the wild-type virus. Lower stabilities of the six-helical bundle structure consisting of S138T peptides and mutant N-HR peptides were shown, but $SC35EK_{S138T}$ was slightly more potent against both resistant viruses compared with the parent peptide.

Using His-tagged N36 or N54 peptides with the V38A or N43D mutation, affinity selection experiments were performed for $SC35EK_{S138X}$ and $T\text{-}20EK_{S138X}$ including 19 components (Table 3 and Table S4, ESI†). Eight SC35EK derivatives captured in significantly high yields all showed potent anti-HIV activity against the V38A mutant. Moderate recovery yields of $SC35EK_{S138E}$ and $SC35EK_{S138Y}$ could result from potential false positive and negative results of the selection, respectively. Although T-20EK derivatives showed lower susceptibility against the V38A mutant in the MAGI assay, an association between the high recovery rate and more potent anti-HIV activity was observed such as S138A, S138I, S138L and S138M derivatives (Figures S3, ESI†). Similar correlations were also obtained against N43D variants. $SC35EK_{S138X}$ and $T\text{-}20EK_{S138X}$ components, which exhibited subnanomolar potent bioactivity, were recovered in moderate to good yields. Overall favorable amino acids for position 138 of the wild-type were useful for designing C-HR peptides against V38A and N43D variants and *vice versa*, suggesting that the essential binding mode around this position is conserved even after acquiring the enfuvirtide resistance.

The structure–activity relationships of Q141 modifications were also investigated (Table 4). All $SC35EK_{Q141X}$ and $T\text{-}20EK_{Q141X}$ peptides except for the Q141P substitution exhibited similar anti-HIV activity in the EC_{50} range of 1.6–3.2 nM and 0.51–4.6 nM, respectively. The significantly low T_m values of Q141P derivatives suggested that the sole proline residue precluded the formation of a bioactive α-helix structure. On the other hand, high potency of the other peptides independent of any other acyclic amino acid substitution at position 141 may be attributable to the lower importance of the Q141 position for the binding affinity between N-HR and C-HR than the S138 position. Among these, Q141I, Q141L and Q141M peptides formed slightly more stable complexes with N36 or N54 and were captured at a relatively higher recovery rate by affinity selection. These substitutions were found to contribute to subnanomolar anti-HIV activity of T-20EK derivatives; however, these peptides were less valid for SC35EK derivatives.

For both S138 and Q141 substitutions, it does not seem possible to distinguish between variations of a few nM in anti-HIV activity by affinity selection. This is particularly the case for the selections regarding less effective residues such as Q141 of SC35EK. In contrast, over a larger range of more than 2 orders of magnitude of affinity variations of T-20EK derivatives, the selection procedure correlated reasonably well with the anti-HIV activity and six-helix bundle stability. In both sequences, highly potent anti-HIV activity peptides were captured in good to high yields.

Conclusions

In conclusion, we have presented an affinity selection-mass spectrometry method to explore novel HIV-1 fusion inhibitors. Predicated on previous findings that the introduction of α-helix-inducible X-EE-XX-KK motifs into inhibitory C-HR peptides should improve peptide solubility in aqueous buffers and disclose the interactive surface to be optimized, a pool of SC35EK and T-20EK derivatives with a single modification at two interactive positions were screened using N-HR peptides corresponding to

wild-type and enfuvirtide-resistant strains. Through the screening of position 138 on C-HR, it was demonstrated that potent anti-HIV peptides could be obtained by substitutions with resistance-related and resistance-independent amino acids. Since a wide variety of synthetic peptides with any unnatural amino acids or peptidomimetics could be employed as candidate components, the system should be applicable to screening for inhibitory α-helix peptides of coiled-coil interactions. The structure–activity relationships of C-HR peptides presented herein may also be suitable in the design of the next-generation of fusion inhibitors. Additionally, since this process is considered to reproduce the evolutionary process of HIV-1 gp41 to select the appropriate folding partners in the presence of fusion inhibitors, the sequence-activity relationships could facilitate understanding of the underlying mechanisms of enfuvirtide resistance.

Acknowledgements

This work was supported by the Science and Technology Incubation Program in Advanced Regions from the Japan Science and Technology Agency, Grants-in-Aid for Scientific Research and Targeted Proteins Research Program from the Ministry of Education, Culture, Sports, Science, and Technology of Japan, and Health and Labour Sciences Research Grants (Research on HIV/AIDS). H.N. is grateful for the JSPS Research Fellowships for Young Scientists.

References

1 T. Matthews, M. Salgo, M. Greenberg, J. Chung, R. DeMasi and D. Bolognesi, *Nat. Rev. Drug Discovery*, 2004, **3**, 215–225.
2 D. C. Chan, C. T. Chutkowski and P. S. Kim, *Proc. Natl. Acad. Sci. U. S. A.*, 1998, **95**, 15613–15617.
3 L. Xu, A. Pozniak, A. Wildfire, S. A. Stanfield-Oakley, S. M. Mosier, D. Ratcliffe, J. Workman, A. Joall, R. Myers, E. Smit, P. A. Cane, M. L. Greenberg and D. Pillay, *Antimicrob. Agents Chemother.*, 2005, **49**, 1113–1119.
4 L. Pérez-Alvarez, R. Carmona, A. Ocampo, A. Asorey, C. Miralles, S. Pérez de Castro, M. Pinilla, G. Contreras, J. A. Taboada and R. Nájera, *J. Med. Virol.*, 2006, **78**, 141–147.
5 D. Eggink, J. P. Langedijk, A. M. Bonvin, Y. Deng, M. Lu, B. Berkhout and R. W. Sanders, *J. Biol. Chem.*, 2009, **284**, 26941–26950.
6 D. Nameki, E. Kodama, M. Ikeuchi, N. Mabuchi, A. Otaka, H. Tamamura, M. Ohno, N. Fujii and M. Matsuoka, *J. Virol.*, 2005, **79**, 764–770.
7 D. C. Chan, D. Fass, J. M. Berger and P. S. Kim, Core structure of gp41 from the HIV envelope glycoprotein, *Cell*, 1997, **89**, 263–273.
8 T. Watabe, Y. Terakawa, K. Watanabe, H. Ohno, H. Nakano, T. Nakatsu, H. Kato, K. Izumi, E. Kodama, M. Matsuoka, K. Kitaura, S. Oishi and N. Fujii, *J. Mol. Biol.*, 2009, **392**, 657–665.
9 K. Izumi, S. Nakamura, H. Nakano, K. Shimura, Y. Sakagami, S. Oishi, S. Uchiyama, T. Ohkubo, Y. Kobayashi, N. Fujii, M. Matsuoka and E. N. Kodama, *Antiviral Res.*, 2010, **87**, 179–186.
10 J. P. Lalezari, N. C. Bellos, K. Sathasivam, G. J. Richmond, C. J. Cohen, R. A. Myers, Jr., D. H. Henry, C. Raskino, T. Melby, H. Murchison, Y. Zhang, R. Spence, M. L. Greenberg, R. A. Demasi and G. D. Miralles, *J. Infect. Dis.*, 2005, **191**, 1155–1163.
11 Y. He, Y. Xiao, H. Song, Q. Liang, D. Ju, X. Chen, H. Lu, W. Jing, S. Jiang and L. Zhang, *J. Biol. Chem.*, 2008, **283**, 11126–11134.
12 K. Izumi, E. Kodama, K. Shimura, Y. Sakagami, K. Watanabe, S. Ito, T. Watabe, Y. Terakawa, H. Nishikawa, S. G. Sarafianos, K. Kitaura, S. Oishi, N. Fujii and M. Matsuoka, *J. Biol. Chem.*, 2008, **284**, 4914–4920.
13 J. Cao, L. Bergeron, E. Helseth, M. Thali, H. Repke and J. Sodroski, *J. Virol.*, 1993, **67**, 2747–2755.
14 W. Shu, J. Liu, H. Ji, L. Radigen, S. Jiang and M. Lu, *Biochemistry*, 2000, **39**, 1634–1642.
15 D. A. Annis, N. Nazef, C. C. Chuang, M. P. Scott and H. M. Nash, *J. Am. Chem. Soc.*, 2004, **126**, 15495–15503.
16 G. C. Adam, C. A. Parish, D. Wisniewski, J. Meng, M. Liu, K. Calati, B. D. Stein, J. Athanasopoulos, P. Liberator, T. Roemer, G. Harris and K. T. Chapman, *J. Am. Chem. Soc.*, 2008, **130**, 16704–16710.
17 S. Oishi, S. Ito, H. Nishikawa, K. Watanabe, M. Tanaka, H. Ohno, K. Izumi, Y. Sakagami, E. Kodama, M. Matsuoka and N. Fujii, *J. Med. Chem.*, 2008, **51**, 388–391.
18 A. Otaka, M. Nakamura, D. Nameki, E. Kodama, S. Uchiyama, S. Nakamura, H. Nakano, H. Tamamura, Y. Kobayashi, M. Matsuoka and N. Fujii, *Angew. Chem., Int. Ed.*, 2002, **41**, 2937–2940.
19 M. Gochin, R. Savage, S. Hinckley and L. Cai, *Biol. Chem.*, 2006, **387**, 477–483.
20 H. Nishikawa, E. Kodama, A. Sakakibara, A. Fukudome, K. Izumi, S. Oishi, N. Fujii and M. Matsuoka, *Antiviral Res.*, 2008, **80**, 71–76.
21 J. K. Judice, J. Y. Tom, W. Huang, T. Wrin, J. Vennari, C. J. Petropoulos and R. S. McDowell, *Proc. Natl. Acad. Sci. U. S. A.*, 1997, **94**, 13426–13430.
22 S. K. Sia, P. A. Carr, A. G. Cochran, V. N. Malashkevich and P. S. Kim, *Proc. Natl. Acad. Sci. U. S. A.*, 2002, **99**, 14664–14669.
23 J. J. Dwyer, K. L. Wilson, D. K. Davison, S. A. Freel, J. E. Seedorff, S. A. Wring, N. A. Tvermoes, T. J. Matthews, M. L. Greenberg and M. K. Delmedico, *Proc. Natl. Acad. Sci. U. S. A.*, 2007, **104**, 12772–12777.

THE JOURNAL OF BIOLOGICAL CHEMISTRY VOL. 285, NO. 49, pp. 38700–38709, December 3, 2010

The N348I Mutation at the Connection Subdomain of HIV-1 Reverse Transcriptase Decreases Binding to Nevirapine*

Received for publication, June 10, 2010, and in revised form, September 7, 2010 Published, JBC Papers in Press, September 27, 2010, DOI 10.1074/jbc.M110.153783

Matthew M. Schuckmann[‡], Bruno Marchand[‡1], Atsuko Hachiya[‡§], Eiichi N. Kodama[¶], Karen A. Kirby[‡], Kamalendra Singh[‡], and Stefan G. Sarafianos[‡2]

From the [‡]Christopher Bond Life Sciences Center, Department of Molecular Microbiology and Immunology, University of Missouri School of Medicine, Columbia, Missouri 65211, [§]AIDS Clinical Center, National Center for Global Health and Medicine (International Medical Center of Japan), 1-21-1 Toyama, Shinjyuku-ku, Tokyo 162-8655, Japan, and [¶]Division of Emerging Infectious Diseases, Tohoku University School of Medicine, 2-1 Seiryocho, Aoba-ku, Sendai 980-8575, Japan

The N348I mutation at the connection subdomain of HIV-1 reverse transcriptase (RT) confers clinically significant resistance to both nucleoside and non-nucleoside RT inhibitors (NNRTIs) by mechanisms that are not well understood. We used transient kinetics to characterize the enzymatic properties of N348I RT and determine the biochemical mechanism of resistance to the NNRTI nevirapine (NVP). We demonstrate that changes distant from the NNRTI binding pocket decrease inhibitor binding (increase $K_{d\text{-NVP}}$) by primarily decreasing the association rate of the inhibitor ($k_{\text{on-NVP}}$). We characterized RTs mutated in either p66 ($p66_{N348I}/p51_{WT}$), p51 ($p66_{WT}/p51_{N348I}$), or both subunits ($p66_{N348I}/p51_{N348I}$). Mutation in either subunit caused NVP resistance during RNA-dependent and DNA-dependent DNA polymerization. Mutation in p66 alone ($p66_{N348I}/p51_{WT}$) caused NVP resistance without significantly affecting RNase H activity, whereas mutation in p51 caused NVP resistance and impaired RNase H, demonstrating that NVP resistance may occur independently from defects in RNase H function. Mutation in either subunit improved affinity for nucleic acid and enhanced processivity of DNA synthesis. Surprisingly, mutation in either subunit decreased catalytic rates (k_{pol}) of $p66_{N348I}/p51_{N348I}$, $p66_{N348I}/p51_{WT}$, and $p66_{WT}/p51_{N348I}$ without significantly affecting affinity for deoxynucleotide substrate ($K_{d\text{-dNTP}}$). Hence, in addition to providing structural integrity for the heterodimer, p51 is critical for fine tuning catalytic turnover, RNase H processing, and drug resistance. In conclusion, connection subdomain mutation N348I decreases catalytic efficiency and causes *in vitro* resistance to NVP by decreasing inhibitor binding.

Human immunodeficiency virus type 1 (HIV-1) reverse transcriptase (RT) converts the viral single-stranded, positive sense RNA genome to a double-stranded DNA, which is integrated into the host genome. To achieve this task, RT possesses multiple enzymatic activities, including both DNA-dependent and RNA-dependent DNA polymerase activities and RNase H activity. RT is a heterodimer composed of 66-kDa (p66) and 51-kDa (p51) subunits. p66 is 560 amino acids long and comprises the spatially distinct polymerase and RNase H domains. The polymerase domain of p66 includes the fingers, palm, and thumb subdomains that resemble a clasping right hand connected to the RNase H domain through the connection subdomain. p51 contains the first 440 amino acids of p66 and is derived by HIV-1 protease-mediated cleavage of an RNase H domain from the p66/p66 homodimer. Because p51 of the heterodimer has no enzymatic function, it has been proposed that its role is simply to provide structural support to p66.

HIV-1 RT has been a prominent target of anti-AIDS therapies. There are two classes of approved drugs that target RT: the nucleoside RT inhibitors (NRTIs)[3] and the non-nucleoside RT inhibitors (NNRTIs). NRTIs mimic deoxynucleotide triphosphate (dNTP) substrates required for DNA synthesis. Once integrated into the nascent viral DNA, NRTIs act as chain terminators because they lack a 3′-OH group required for formation of a phosphodiester bond with the incoming nucleotide (1, 2). On the other hand, NNRTIs are non-competitive RT inhibitors with respect to either dNTP or nucleic acid substrates and have been proposed to interfere with the chemical step of DNA synthesis by altering the precise geometry of the polymerase active site and by restricting the mobility of the p66 thumb (3–9). NNRTIs bind at the NNRTI binding pocket (NNIBP), a hydrophobic pocket at the base of the p66 thumb and close (~10 Å) to the polymerase active site, formed primarily by residues from p66 and Glu-138 from p51. NNRTI binding results in conformational changes that shift the "primer grip" and overextend the p66 thumb (10). Both classes of drugs have been successfully used as key components of highly active antiretroviral therapies in combination with protease, integrase, and entry inhibitors. However, as is the case with all anti-AIDS drugs, prolonged use inevitably leads to the emergence of drug-resistant HIV strains.

RT uses two main strategies to develop NRTI resistance. The first strategy involves a selective interference with the incorpo-

* This work was supported, in whole or in part, by National Institutes of Health Grants AI076119 and AI074389 (to S. G. S.) and AI079801. This work was also supported by a grant from the Korea Food and Drug Administration and the Ministry of Knowledge and Economy, Bilateral International Collaborative Research and Development Program, Republic of Korea.

[1] Recipient of the American Foundation for AIDS Research Mathilde Krim Fellowship.

[2] To whom correspondence should be addressed: Christopher Bond Life Sciences Center, Dept. of Molecular Microbiology and Immunology, University of Missouri School of Medicine, 401 Bond Life Sciences Center, 1201 E. Rollins St., Columbia, MO 65211. Tel.: 573-882-4338; E-mail: sarafianoss@missouri.edu.

[3] The abbreviations used are: NRTI, nucleoside RT inhibitor; NNRTI, non-nucleoside RT inhibitor; NVP, nevirapine; NNIBP, NNRTI binding pocket; AZT, azidothymidine; CSM, connection subdomain mutation.

ration of NRTIs into viral DNA (11–15). The second mechanism involves enhanced excision and removal of the chain terminator from the 3′-end of the blocked primer using ATP as a nucleophile (16–18). Unblocking the primer terminus frees the reactive hydroxyl group at the 3′-end of the primer and allows for continued DNA synthesis. Typically, NRTI resistance mutations are found at the NRTI- or ATP-binding sites (19–21).

NNRTI resistance is caused by mutations at, or close to, the NNIBP (5) that have been shown to reduce inhibitor binding through loss or change of contacts (22–25), through steric interactions (25, 26), or by interfering with the entry of the NNRTI because they change interactions at the entrance of the NNIBP (27, 28).

Until recently, almost all clinically relevant NRTI and NNRTI resistance mutations were found at the p66 fingers and palm subdomains. Lately, an increasing number of mutations at the connection subdomain and RNase H domain have been shown to enhance resistance to azidothymidine (AZT) (29, 30). We and others have recently shown that N348I is the first clinically significant single amino acid mutation found to confer resistance to multiple members of both NRTI and NNRTI classes of inhibitors (31–33). N348I often emerges as a result of AZT- and/or didanosine-containing therapy and is found in combination with AZT excision-enhancing mutations (32, 34). N348I is not a polymorphism; it appears in ~10% of treatment-experienced individuals compared with less than 1% in treatment-naïve patients (31). N348I has also been detected at a high frequency in patients receiving AZT/lamivudine (2′,3′-dideoxy-3′-thiacytidine) treatment, and it has been recently suggested that N348I compensates for the antagonism between M184V and excision-enhancing mutations (35, 36). In cell culture experiments, HIV harboring N348I RT (HIV-1_{N348I}) is resistant to NRTIs, including AZT and didanosine, and when in combination with excision-enhancing mutations enhances resistance to tenofovir (31, 32, 37). HIV-1_{N348I} is also resistant to NNRTIs, such as nevirapine (NVP), and to a lesser extent to delavirdine (31–33). When in combination with the NNRTI resistance mutation Y181C, N348I enhances resistance to the second generation NNRTI etravirine (37).

Several studies have focused on the mechanism by which CSMs confer resistance to NRTIs. Nikolenko *et al.* (30, 38) proposed that a number of CSMs increase AZT resistance by reducing template RNA degradation, thereby preserving the RNA template and providing additional time for RT to excise AZT monophosphate. Yap *et al.* (31) showed that N348I reduces the rate of RNA template degradation by RT in either a WT background or in the presence of excision-enhancing AZT resistance mutations. Ehteshami *et al.* (39) proposed that CSMs N348I and A360V enhance resistance to AZT through both RNase H-dependent and -independent mechanisms. Specifically, addition of the CSMs N348I and A360V to the AZT-resistant M41L/D67N/T215Y RT enhanced AZT resistance by causing preservation of AZT-terminated RNA/DNA that can be unblocked by RT with CSMs (39).

The mechanism by which CSMs confer resistance to NNRTIs is largely unknown. Moreover, the effect of N348I on the biochemical aspects of DNA synthesis is also not well understood. Here we resolved the mechanism of NVP resistance using pre-steady state kinetics analysis to quantify NVP binding and dissociation from wild-type (WT) and N348I enzymes. We also determined how Ile-348 in p66 (Ile-348_{p66}) or p51 (Ile-348_{p51}) affects other enzymatic properties of RT relevant to drug resistance, including the efficiency of DNA polymerization, RNase H activity, processivity of DNA synthesis, and affinity for various substrates.

EXPERIMENTAL PROCEDURES

Enzymes and Nucleic Acids—We prepared subunit-specific RT mutants by expressing the two subunits from a single plasmid, allowing *in situ* folding and yielding proteins of superior quality compared with those obtained from reconstitution of separately expressed RT subunits. In our experience, this method of RT expression is a critical factor for optimizing transient kinetics and crystallographic data. The p66 and p51 sequences of RT (BH-10) were cloned in the pETDuet-1 vector (Novagen) using restriction sites PpumI and SacI for p51 and SacII and AvrII for p66. To produce mutant RT, sequences coding for p66 and p51 were independently subcloned and mutated using the QuikChange mutagenesis kit (Stratagene) before being sequentially cloned into a pETDuet-1 vector. Sequences coding for a hexahistidine tag and the 3C protease recognition sequence were added at the N terminus of p51. RT enzymes were expressed in BL21 *Escherichia coli* (Invitrogen) and purified by nickel affinity chromatography and mono Q anion exchange chromatography as described previously (40). Oligonucleotides were purchased from Integrated DNA Technologies (Coralville, IA). All reactions, with the exception of NVP susceptibility and RNase H assays, used Td_{31}/Cy3-Pd_{18} as a template/primer. The Td_{31}/Cy3-Pd_{18} template sequence was 5′-CCATAGCTAGCATTGGTGCTCGAACAGTGAC-3′ (Td_{31}), and the 5′ Cy3-labeled DNA primer sequence was 5′-Cy3-GTCACTGTTCGAGCACCA-3′ (Cy3-Pd_{18}). For the NVP susceptibility assays, a 100-base-long template (T_{100}; described in Ref. 40) annealed to the Pd_{18} primer was used. For the RNase H assays, a 22-base pair duplex (Cy3-Tr_{35}/Pd_{22}) consisting of a 5′ Cy3-labeled RNA template (Cy3-Tr_{35}) of the sequence 5′-Cy3-GGAAAUCUCUAGCAGUGGCGCCCGAACAGGGACCU-3′ annealed to a DNA primer (Pd_{22}) of the sequence 5′-AGGTCCCTGTTCGGGCGCCACT-3′ was used (39). Primers were annealed to templates at concentrations corresponding to a 1:3 molar ratio. Deoxynucleotide triphosphates and dideoxynucleotide triphosphates were purchased from Fermentas (Glen Burnie, MD). The concentrations of nucleotides and nucleic acids were calculated spectrophotometrically based on absorption at 260 nm.

Active Site Titration and Determination of $K_{d\text{-}DNA}$—We determined the active site concentrations of RT preparations using pre-steady state burst experiments. We preincubated a fixed concentration of RT (40 nM; determined by absorbance measurements) in RT buffer (50 mM NaCl and 50 mM Tris-HCl, pH 7.8) with increasing concentrations of Td_{31}/Cy3-Pd_{18} followed by rapidly mixing with a solution of $MgCl_2$ (5 mM) and dATP (50 μM) in RT buffer (41) using an RQF-3 rapid quench-flow instrument (KinTek Corp., Austin, TX) (all values are final concentrations). Reaction mixtures were then incubated at 37 °C for times spanning 0.005–5 s before quenching with

EDTA (50 mM). Reaction products were resolved under denaturing conditions in polyacrylamide-urea DNA gels and quantitated by phosphorimaging and densitometry using Multi Gauge V3.0 (FujiFilm). First the amounts of extended primer (P) were plotted against time with GraphPad Prism 4, and the data were fit to the following biphasic equation,

$$P = A(1 - e^{-k_{obs}t}) + k_{ss}t \quad \text{(Eq. 1)}$$

where A is the amplitude of the burst phase that represents the enzyme-DNA complex at the start of the reaction, k_{obs} is the observed burst rate constant for dNTP incorporation, k_{ss} corresponds to the steady state rate constant, and t is the reaction time. Next, the active site concentration and template/primer dissociation constant ($K_{d\text{-DNA}}$) were determined by plotting the amplitude (A) against template/primer concentration. The data were fit by non-linear regression to a quadratic equation,

$$A = 0.5((K_{d\text{-DNA}} + [RT] + [DNA]) - \sqrt{0.25(K_{d\text{-DNA}} + [RT] + [DNA])^2 - ([RT][DNA])}) \quad \text{(Eq. 2)}$$

where [RT] is the concentration of actively binding polymerase molecules. Subsequent transient state biochemical experiments were performed using corrected active site concentrations.

Pre-steady State Kinetics of dNTP Incorporation—The optimal polymerase rates were obtained by pre-steady state kinetics analysis using single nucleotide incorporation assays. A solution containing RT (30 nM), Td_{31}/Cy3-Pd_{18} (30 nM), and EDTA (0.5 mM) in RT buffer was mixed with a solution of $MgCl_2$ (5 mM) and dATP (0.5–75 μM) for reaction times ranging between 0.005 and 5 s before quenching with EDTA (50 mM). Reaction products were resolved and quantitated as described above. Burst phase incorporation rates and substrate affinities at individual dATP concentrations were obtained from fitting the data to the burst equation (Equation 1). To determine optimal rates of dNTP incorporation (k_{pol}) and dNTP binding to the enzyme-DNA complex ($K_{d\text{-dATP}}$), observed burst rates (k_{obs}) were fit to the following hyperbolic equation.

$$k_{obs} = (k_{pol}[dNTP])/(K_{d\text{-dNTP}} + [dNTP]) \quad \text{(Eq. 3)}$$

Single Turnover Processivity Assays—Processivity assays were conducted under single turnover conditions as described by Patel *et al.* (42). Solutions containing Td_{31}/Cy3-Pd_{18} (20 nM), WT (40 nM) or mutant enzyme (60 nM $p66_{N348I}/p51_{N348I}$), and EDTA (0.5 mM) in RT buffer were mixed with solutions containing dNTPs (50 μM) and $MgCl_2$ (5 mM) for varying times (0.05–5 s) before quenching with EDTA (50 mM). Reaction products were resolved and quantitated as described above. To obtain the rate of Pd_{18} extension, results were plotted using a one-phase exponential decay equation,

$$P = A_0(e^{-k_{app}t}) + C \quad \text{(Eq. 4)}$$

where k_{app} is the apparent rate of product (P) formation, A_0 is the amplitude, t is time, and C is a constant. The rates of nucleotide incorporation at individual positions along the template were obtained by fitting data to a double exponential equation,

$$P = A(1 - e^{-k_1t}) + (e^{-k_2t}) + C \quad \text{(Eq. 5)}$$

where A is the concentration of 19-mer or higher length products, k_1 is the rate of product generation, k_2 is the rate of subsequent product elongation, and C is a constant.

RNase H Assays—RNase H assays were performed by incubating RNA/DNA duplex Cy3-Tr_{35}/Pd_{22} (100 nM) with RT (200 nM) in RT buffer at 37 °C with $MgCl_2$ (6 mM). Reactions were quenched after incubation (1–8 min) with equal volumes of 99% formamide containing trace amounts of bromphenol blue. Reaction products were resolved in denaturing polyacrylamide-urea DNA gels and quantitated as described above. The primary RNase H cleavage product is mainly 18 nucleotides from the 3′-end of the DNA primer (−18 nucleotides), and the secondary cleavage product is mainly 12 nucleotides from the 3′-end of the primer (−12 nucleotides) as reported previously (39, 43).

Nevirapine Susceptibility Assays—Drug susceptibility steady state assays were carried out by measuring the extension of Td_{100}/Pd_{18} in the presence of increasing concentrations of NVP. Reactions of 50 μl containing RT (2 nM), $MgCl_2$ (5 mM), Td_{100}/Pd_{18} (10 nM), and dNTPs (0.8 μM of each with 0.5 μCi/nmol α-^{32}P-labeled dTTP) in RT buffer were initiated by the addition of $MgCl_2$ (6 mM), incubated at room temperature for 15 min, and terminated by the addition of EDTA (50 mM). Reaction products were then passed through a charged nylon filter using a vacuum manifold apparatus (Whatman, GE Healthcare). Extended primers, radiolabeled by the incorporation of [^{32}P]dTMP, bound to the membrane, whereas the unincorporated [α-^{32}P]dTTP was filtered through. Radioactive filters were exposed to phosphor screens followed by phosphorimaging and analysis using the Multi Gauge V3.0 software (FujiFilm). Dose-response curves of triplicate samples were plotted using GraphPad Prism 4 to determine IC_{50} values for NVP.

Gel-based NVP susceptibility assays were performed using Td_{31}/Cy3-Pd_{18} or Tr_{31}/Cy3-Pd_{18} (RNA template of corresponding sequence). RT (20 nM) was preincubated with increasing concentrations of NVP in RT buffer for 5 min at 37 °C before the addition of template/primer (60 nM), dNTPs (1 μM), and $MgCl_2$ (5 mM). Reactions were allowed to proceed for 5 min at 37 °C before being quenched with EDTA (50 mM). Reaction products were resolved on denaturing polyacrylamide-urea DNA gels, and fluorescent bands corresponding to full-extension products were quantified as described above. IC_{50} values were derived from dose-response curves using GraphPad Prism 4.

Nevirapine Binding Assays—Solutions of RT (30 nM active sites), Td_{31}/Cy3-Pd_{18} (30 nM), and EDTA (5 mM) in RT buffer were incubated with various concentrations of NVP for 10 min at room temperature before initiating reactions with $MgCl_2$ (0.5 mM) and saturating dATP (100 μM). Reactions were allowed to proceed for times between 0.005 and 5 s before quenching with EDTA (50 mM). Reaction products were fit to the burst equation (Equation 1) to calculate burst amplitudes (A) for each data set. Burst amplitudes were then fit to the following hyperbolic equation (44) to determine the dissociation constant for NVP ($K_{d\text{-NVP}}$),

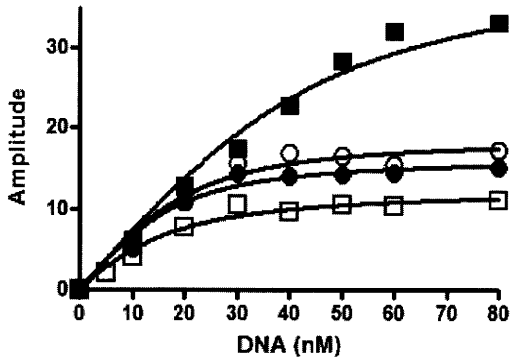

FIGURE 1. **Calculation of dissociation constants of WT and N348I mutant RTs for nucleic acid ($K_{d\text{-DNA}}$).** Enzymes (40 nM; as determined by absorbance measurements at 280 nm) were preincubated with increasing concentrations of Td_{31}/Cy3-Pd_{18} duplex DNA. The RT-DNA complex was rapidly mixed with $MgCl_2$ and dATP and incubated for times spanning from 0.005 to 5 s before quenching with EDTA (50 mM final concentration). The burst amplitudes were calculated for each concentration of DNA by fitting the corresponding time courses to the burst equation (see "Experimental Procedures"). The amplitudes were plotted as a function of the DNA concentrations and fit to a quadratic equation. The fit of the data yielded the following K_d values for each enzyme: WT (■), $K_{d\text{-DNA}}$ = 12.5 nM; $p66_{N348I}/p51_{N348I}$ (□), $K_{d\text{-DNA}}$ = 9.9 nM; $p66_{N348I}/p51_{WT}$ (●), $K_{d\text{-DNA}}$ = 4.8 nM; and $p66_{WT}/p51_{N348I}$ (○), $K_{d\text{-DNA}}$ = 5.4 nM.

TABLE 1
Pre-steady state RT kinetics

	$K_{d\text{-DNA}}$	k_{pol}	$K_{d\text{-dATP}}$	$k_{pol}/K_{d\text{-dATP}}$
	nM	s^{-1}	μM	$\mu M^{-1} s^{-1}$
WT	12.5	24.4 ± 0.9	1.3 ± 0.4	18.8
$p66_{N348I}/p51_{N348I}$	9.9	5.7 ± 0.3	1.0 ± 0.3	5.7
$p66_{N348I}/p51_{WT}$	4.8	8.6 ± 0.4	0.9 ± 0.2	9.6
$p66_{WT}/p51_{N348I}$	5.4	8.4 ± 0.3	0.8 ± 0.4	10.5

$$A = [RT] - \left(\frac{[RT][I]}{K_{d\text{-NVP}} + [I]}\right) + C \quad \text{(Eq. 6)}$$

where [RT] is the concentration of actively binding polymerase molecules, [*I*] is the concentration of inhibitor, and *C* is a constant.

The apparent rate of NVP binding to RT ($k_{app\text{-NVP}}$) was obtained by premixing a solution of RT (30 nM) and Td_{31}/Cy3-Pd_{18} (30 nM) in RT buffer with saturating NVP (40 μM) for increasing amounts of time (0.2–5 s). Reactions were then initiated by addition of $MgCl_2$ (5 mM) and saturating dATP (50 μM), allowed to proceed for 0.2 s, and quenched with EDTA (250 mM). Reaction products were resolved and quantitated as described above and plotted with GraphPad Prism 4 using an equation for one-phase exponential decay,

$$P = A_0(e^{-k_{app\text{-NVP}}t}) + C \quad \text{(Eq. 7)}$$

where *P* is the reaction product, A_0 is the amount of product in the absence of NVP, *t* is the preincubation time with NVP before addition of $MgCl_2$/dATP, and *C* is a constant.

The $k_{app\text{-NVP}}$ values obtained were next inserted into the following equation to derive the NVP association constant ($k_{on\text{-NVP}}$) (8).

$$k_{app\text{-NVP}} = k_{on\text{-NVP}}([NVP] + K_{d\text{-NVP}}) \quad \text{(Eq. 8)}$$

The $k_{on\text{-NVP}}$ and $K_{d\text{-NVP}}$ values were then used to calculate the NVP dissociation rate ($k_{off\text{-NVP}}$) through the following equation.

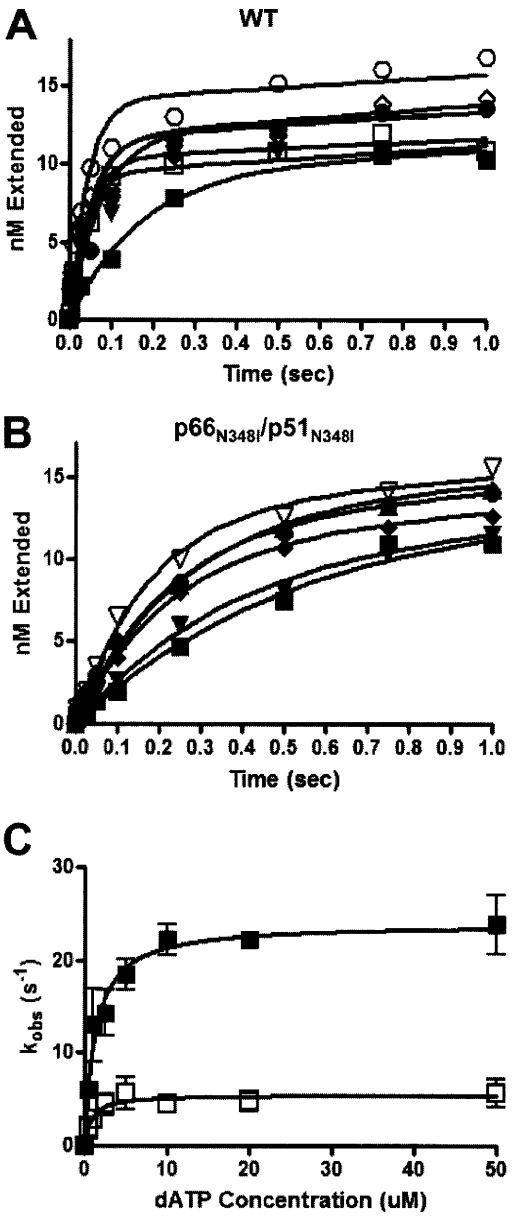

FIGURE 2. Pre-steady state kinetics of dATP incorporation by WT (*A*) and $p66_{N348I}/p51_{N348I}$ (*B*) RTs are shown. 30 nM RT (active sites) were preincubated with 30 nM Td_{31}/Cy3-Pd_{18}. Reactions were initiated by adding 10 mM $MgCl_2$ plus varying concentrations of dATP (0.5 μM, ■; 1 μM, ▼; 2.5 μM, ●; 10 μM, ◇; 20 μM, □; and 50 μM, ○) before being quenched with EDTA. All stated concentrations are the final concentrations after mixing. *C*, pre-steady state burst dependence of dATP incorporation by WT (■) or $p66_{N348I}/p51_{N348I}$ (□) RTs. The first turnover rates were obtained from the burst phases and were then fit to a quadratic equation as a function of dATP concentration. The WT enzyme displayed a $K_{d\text{-dATP}}$ of 1.3 ± 0.4 μM and a maximum incorporation rate of 24.4 ± 0.9 s^{-1}. The double mutant RT ($p66_{N348I}/p51_{N348I}$) showed a similar $K_{d\text{-dATP}}$ of 1.0 ± 0.3 μM and a reduced maximum incorporation rate of 5.7 ± 0.3 s^{-1}. *Error bars* represent the standard deviation between results of at least three experiments.

$$K_{d\text{-NVP}} = k_{off\text{-NVP}}/k_{on\text{-NVP}} \quad \text{(Eq. 9)}$$

Molecular Modeling—A molecular model of $p66_{N348I}/p51_{N348I}$ was generated using starting protein coordinates from the crystal structure of HIV-1 RT in complex with NVP (Protein Data Bank code 1VRT) (3). The coordinates were initially processed by the Protein Preparation tool (Schrödinger Molecular Modeling Suite, New York, NY), which deletes unwanted

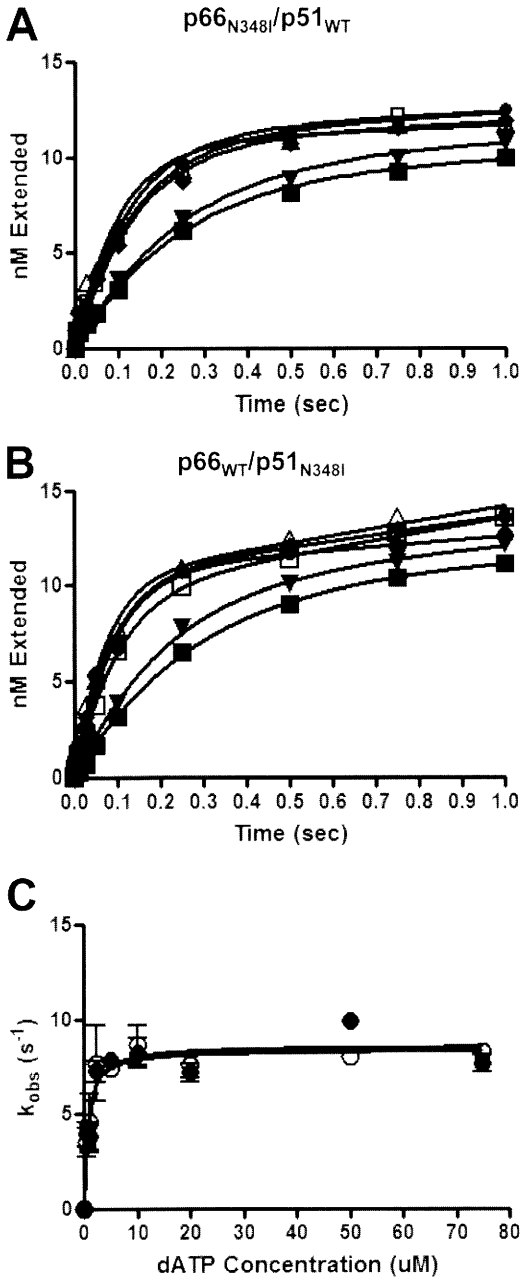

FIGURE 3. Pre-steady state kinetics of dATP incorporation by subunit-specific mutant enzymes $p66_{N348I}/p51_{WT}$ (*A*) and $p66_{WT}/p51_{N348I}$ (*B*) are shown. 30 nM RT (concentration of active sites) and 30 nM $Td_{31}/Cy3\text{-}Pd_{18}$ were preincubated in RT buffer. Reactions were initiated by adding 10 mM $MgCl_2$ plus increasing concentrations of dATP (0.5 μM, ■; 1 μM, ▼; 2.5 μM, ●; 10 μM, ◆; 20 μM, □; and 50 μM, ○) and quenched with EDTA. *C*, pre-steady state burst dependence of dATP incorporation by the site-directed mutant enzymes. $p66_{N348I}/p51_{WT}$ (●) showed a $K_{d\text{-dATP}}$ of 0.9 ± 0.2 μM and a maximum incorporation rate of 8.6 ± 0.4 s^{-1}. $p66_{WT}/p51_{N348I}$ (○) showed a $K_{d\text{-dATP}}$ of 0.8 ± 0.4 μM and a maximum incorporation rate of 8.4 ± 0.3 s^{-1}. *Error bars* represent the standard deviation between results of at least three experiments.

water molecules, sets charges and atom type of metal ions, corrects misoriented Gln and Asn residues, and optimizes hydrogen atom orientations. Amino acid side chains were substituted as needed using the Maestro software (Schrödinger Molecular Modeling Suite). To ensure that any observed changes in the structure of the mutant were not due to the protocols used, the WT structure was also treated in parallel using the same protocols. Molecular dynamics simulations of the WT and $p66_{N348I}/p51_{N348I}$ models were performed to obtain optimally stable structures using the software Impact, interfaced with Maestro, at constant temperature, and the OPLS_2005 force field. The molecular dynamics simulations were performed for 1000 steps with 0.001-ps intervals. The temperature relaxation time was 0.01 ps. The Verlet integration algorithm was used in the simulations. Visualization of the molecules, comparisons, and figure preparation were carried out using PyMOL.

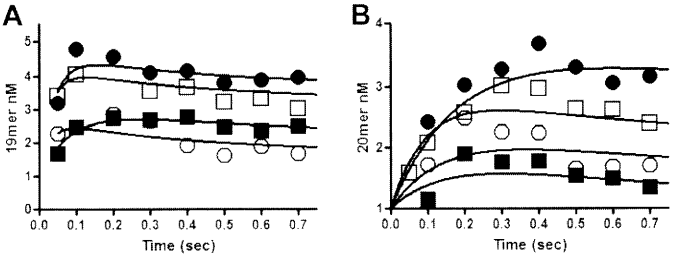

FIGURE 4. **Single turnover processivity assays.** 20 nM $Td_{31}/Cy3\text{-}Pd_{18}$ was combined with 40 nM RT in RT buffer before rapidly mixing with saturating NVP (20 μM) for varying incubation times (0.05–1 s). Next, $MgCl_2$ (10 mM) and saturating dATP (50 μM) were rapidly added, and reactions were allowed to proceed for 200 ms before quenching with EDTA. Extension of the 18-mer primer into 19-mer (*A*), 20-mer (*B*), and 21-mer products (not shown) by WT (■), $p66_{N348I}/p51_{N348I}$ (□), $p66_{N348I}/p51_{WT}$ (●), or $p66_{WT}/p51_{N348I}$ (○) was quantified to determine rates of product appearance and subsequent processive extension of those products.

TABLE 2
Single turnover processivity (-fold change over WT)

	19-mer	20-mer	21-mer	Average
WT	1	1	1	1
$p66_{N348I}/p51_{N348I}$	3.3	1.5	1.1	2.0
$p66_{N348I}/p51_{WT}$	1.8	0.89	1.1	1.3
$p66_{WT}/p51_{N348I}$	2.9	0.76	1.2	1.6

RESULTS

Effect of N348I on Enzyme-Template/Primer Complex Formation—We determined the effect of N348I on DNA/DNA binding affinity using a pre-steady state kinetics assay where we titrated the amount of nucleic acid that can be bound to, and extended by, RT (Fig. 1). These experiments showed the $K_{d\text{-DNA}}$ for the double mutant ($p66_{N348I}/p51_{N348I}$) to be 9.9 nM, slightly lower than that for WT (12.5 nM; Table 1). Subunit-specific experiments were performed to further dissect the effect of the mutation in either RT subunit. These experiments determined the $K_{d\text{-DNA}}$ values for $p66_{N348I}/p51_{WT}$ and $p66_{WT}/p51_{N348I}$ to be 4.8 and 5.4 nM, respectively. Hence, the presence of either $Ile\text{-}348_{p66}$ or $Ile\text{-}348_{p51}$ resulted in an increased affinity for double-stranded DNA. These results were consistent with gel shift assays, which also showed that the mutant enzymes bind DNA/DNA and RNA/DNA oligonucleotides slightly more efficiently than does WT RT (data not shown).

Pre-steady State Kinetics of Single Nucleotide Incorporation—Kinetics of pre-steady state dATP incorporation were determined as described previously (8). Both WT and $p66_{N348I}/p51_{N348I}$ exhibited a biphasic pattern of nucleotide incorporation (initial burst phase followed by steady state phase; Fig. 2). The kinetics constants (k_{pol}, $K_{d\text{-dATP}}$, and catalytic efficiency or $k_{pol}/K_{d\text{-dATP}}$) estimated from pre-steady state kinetic analyses are shown in Table 1. The $p66_{N348I}/p51_{N348I}$ enzyme displayed a ~4-fold decrease in k_{pol} relative to WT without a significant

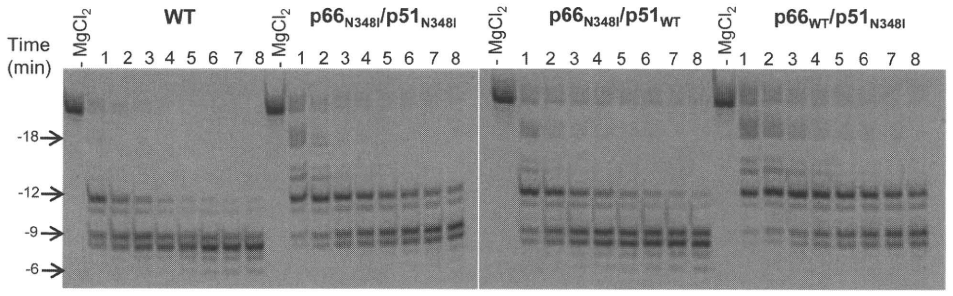

FIGURE 5. **Effect of mutations on RNase H Activity.** 100 nM Cy3-Tr_{35}/Pd_{22} DNA/RNA was incubated with 200 nM active RT for varying times (1–8 min) at 37 °C in RT buffer. Reactions were quenched with equal volumes of 99% formamide containing trace amounts of bromphenol blue. The control (no added $MgCl_2$) shows the full-length, uncleaved RNA template. The cleavage positions relative to the 3′ terminus of the DNA primer are indicated to the *left* of the gel images.

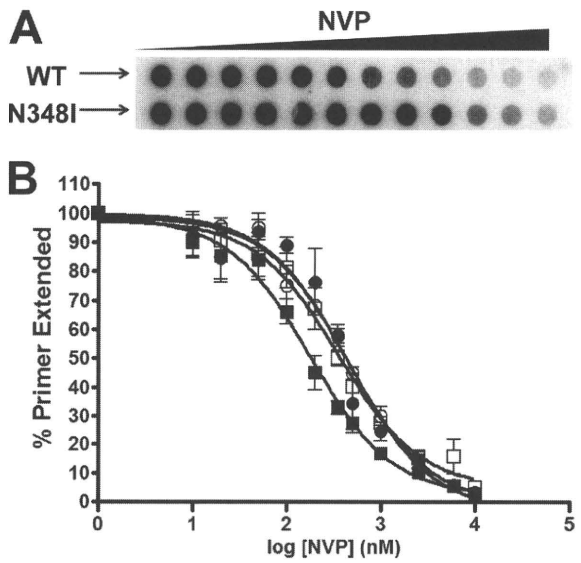

FIGURE 6. *A*, filter binding assay for NVP susceptibility. DNA/DNA duplex (10 nM) was incubated with HIV-1 RT (2 nM) in RT buffer in the presence of varying amounts of inhibitor. All dNTPs were present at a final concentration of 0.8 μM each with 0.5 μCi of [α-^{32}P]dTTP. Reactions were initiated by the addition of 6 mM $MgCl_2$ and quenched with EDTA. Products were passed through a charged nylon filter using a vacuum manifold apparatus. *B*, WT (■) RT displayed an IC_{50} of 187 ± 3 nM, and $p66_{N348I}/p51_{N348I}$ (□) displayed an IC_{50} of 356 ± 3 nM. In the case of the subunit-specific mutants, the $p66_{N348I}/p51_{WT}$ (●) enzyme displayed an IC_{50} of 401 ± 4 nM, and the $p66_{WT}/p51_{N348I}$ (○) RT showed an IC_{50} of 448 ± 2 nM. *Error bars* represent the standard deviation between results of at least three experiments.

TABLE 3
NVP susceptibility (-fold resistance)

	Filter binding assay, DNA/DNA	Gel-based assay	
		DNA/DNA	RNA/DNA
WT	1	1	1
$p66_{N348I}/p51_{N348I}$	1.9	2.7	2
$p66_{N348I}/p51_{WT}$	2.1	1.9	2
$p66_{WT}/p51_{N348I}$	2.4	3.1	2.7

change in $K_{d\text{-dATP}}$ (Table 1). Hence, WT RT had a catalytic efficiency ($k_{pol}/K_{d\text{-dATP}}$) over 3-fold greater than the N348I double mutant enzyme. Interestingly, the presence of Ile-348_{p66} or Ile-348_{p51} did not affect affinity for dATP but did decrease the turnover number (k_{pol}) (Figs. 2 and 3 and Table 1). Moreover, the decreases in catalytic efficiencies for Ile-348_{p66} and Ile-348_{p51} appear to be additive (Table 1).

Single Turnover Processivity Assays—We applied a single turnover processivity assay developed by Patel *et al.* (42) to quantify relative processivities of DNA polymerization (Fig. 4). In this assay, we monitored rates of consecutive nucleotide incorporations under single turnover conditions where enzyme dissociation from the nucleic acid prohibits elongation of the primer strand. The rate of single nucleotide incorporation (k_1) and the rate of processive DNA synthesis (k_2) were calculated at several template positions for each enzyme. The ratio of the rate of processive DNA synthesis to the rate of nucleotide incorporation (k_2/k_1) is referred to here as the processivity index. Our experiments clearly demonstrated a reproducible ~2-fold enhancement in processivity for $p66_{N348I}/p51_{N348I}$ relative to the WT enzyme (Table 2). Moreover, both Ile-348_{p66} and Ile-348_{p51} slightly enhanced processivity. These results were consistent with trap-based experiments performed in our laboratory (data not shown) and by others (39).

RNase H Assays—To determine whether Ile-348_{p66} or Ile-348_{p51} alters the RNase H activity of RT, we monitored time course RNase H cleavages of 5′-Cy3-RNA/DNA. Cleavage patterns produced by WT and $p66_{N348I}/p51_{N348I}$ are similar to those reported previously (39). The primary RNA cleavage typically occurs 17–18 nucleotides upstream from the polymerase active site positioned at the 3′ primer end. The enzyme then repositions to make a secondary cleavage ~12 nucleotides upstream from the 3′ primer end. Over time, the secondary cleavage products are further processed into increasingly smaller fragments. Our experiments demonstrated that both the primary and the secondary cleavage activities of $p66_{N348I}/p51_{N348I}$ were slower than those noted for WT (Fig. 5). At extended incubation times, we observed the accumulation of secondary cleavage products in the case of $p66_{N348I}/p51_{N348I}$, consistent with a more significant impairment of postsecondary cleavages compared with the effects on primary cleavage (Fig. 5). Interestingly, the secondary cleavage products in the case of $p66_{N348I}/p51_{WT}$ appear comparable with WT. However, $p66_{WT}/p51_{N348I}$ generated cleavage products similar to those of the double mutant $p66_{N348I}/p51_{N348I}$ RT.

Nevirapine Susceptibility—Drug susceptibility assays have shown that viruses harboring the N348I RT mutation are resistant to NVP (31, 32). We found the NVP resistance of N348I to be higher at the virus level in cell-based assays than with assays using purified RT enzymes (Fig. 6), similar to the results reported by Yap *et al.* (31) and Hachiya *et al.* (32). Our *in vitro* filter binding and gel-based NVP susceptibility assays using DNA/DNA or RNA/DNA substrates showed that $p66_{N348I}/p51_{N348I}$ is ~2–3-fold resistant to NVP relative to WT (Fig. 6 and Table 3). Interestingly, both Ile-348_{p66} and Ile-348_{p51} conferred NVP resistance in gel-based and filter binding assays using either DNA/DNA or RNA/DNA substrates (~2-fold resistance for $p66_{N348I}/p51_{WT}$ and ~3-fold resistance for $p66_{WT}/p51_{N348I}$) (Table 3).

Determination of $K_{d\text{-NVP}}$—The suppression of polymerization burst amplitude by NVP represents the amount of inhibi-

N348I Decreases HIV-1 RT Binding to Nevirapine

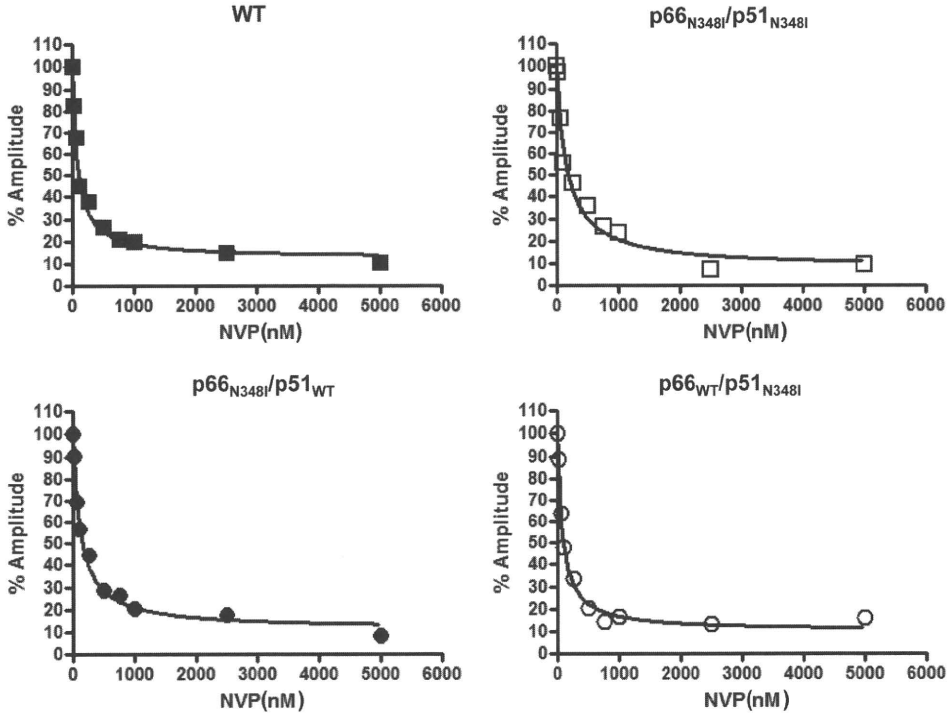

FIGURE 7. **Determination of NVP dissociation equilibria ($K_{d\text{-NVP}}$).** Single nucleotide dATP incorporation assays were performed under pre-steady state conditions. RT (30 nM active sites) was incubated with 30 nM Td_{31}/Cy3-Pd_{18} and varying concentrations of NVP. Reactions were initiated by adding $MgCl_2$ (10 mM) plus saturating dATP before being quenched with EDTA. The burst amplitudes for RT WT and $p66_{N348I}/p51_{N348I}$ were plotted against NVP concentration and fit to a hyperbolic equation (see "Experimental Procedures"). The $K_{d\text{-NVP}}$ for WT (■) was determined to be 0.08 ± 0.01 μM, and the $K_{d\text{-NVP}}$ for $p66_{N348I}/p51_{N348I}$ (□) was 0.16 ± 0.04 μM. The subunit-specific mutant enzyme $p66_{N348I}/p51_{WT}$ (●) had a $K_{d\text{-NVP}}$ of 0.12 ± 0.02 μM, and the $K_{d\text{-NVP}}$ of $p66_{WT}/p51_{N348I}$ (○) was 0.07 ± 0.01 μM.

TABLE 4

Kinetics of NVP binding

-Fold change relative to WT is in parentheses.

	$K_{d\text{-NVP}}$	$k_{app\text{-NVP}}$	$k_{on\text{-NVP}}$	$k_{off\text{-NVP}}$
	μM	s^{-1}	$10^4\ M^{-1}\ s^{-1}$	s^{-1}
WT	0.08 ± 0.01 (1)	2.3 ± 0.6 (1)	5.7 (1)	0.005 (1)
$p66_{N348I}/p51_{N348I}$	0.16 ± 0.04 (2)	1.3 ± 0.4 (0.6)	3.4 (0.6)	0.005 (1)
$p66_{N348I}/p51_{WT}$	0.12 ± 0.02 (1.5)	2.0 ± 0.6 (0.9)	5.0 (0.9)	0.006 (1.2)
$p66_{WT}/p51_{N348I}$	0.07 ± 0.01 (1)	0.6 ± 0.1 (0.25)	1.5 (0.3)	0.001 (0.2)

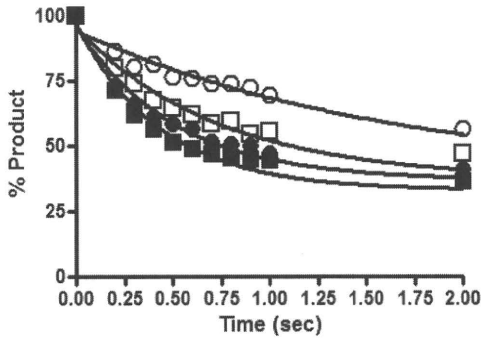

FIGURE 8. **NVP binding kinetics: apparent binding rates of nevirapine ($k_{app\text{-NVP}}$).** RT (30 nM active sites) was first incubated in RT buffer with 30 nM Td_{31}/Cy3-Pd_{18}. This solution was rapidly mixed with an equal volume of saturating NVP (40 μM) for the indicated times before then being mixed with saturating dATP (50 μM) and $MgCl_2$ (10 mM). The reactions were quenched with 250 mM EDTA, pH 8.0. Reaction products were fit to a single exponential decay equation to obtain observed binding rates. The k_{app} for RT WT (■) was 2.3 ± 0.6 s^{-1}, the k_{app} for $p66_{N348I}/p51_{N348I}$ (□) was 1.3 ± 0.4 s^{-1}, the k_{app} for $p66_{N348I}/p51_{WT}$ (●) was 2.0 ± 0.6 s^{-1}, and the k_{app} for $p66_{WT}/p51_{N348I}$ (○) was 0.6 ± 0.1 s^{-1}.

tor bound to the RT-DNA complex (8). We therefore determined the dissociation constant of NVP ($K_{d\text{-NVP}}$) from various RTs by measuring the effect of the inhibitor on the pre-steady state burst phase of polymerization as described by Johnson and co-workers (8). Burst amplitude suppression values were plotted using a hyperbolic equation to obtain $K_{d\text{-NVP}}$ (Fig. 7). The $K_{d\text{-NVP}}$ for WT RT was 0.08 μM, whereas $K_{d\text{-NVP}}$ for $p66_{N348I}/p51_{N348I}$ was 2-fold greater (0.16 μM) (Fig. 7 and Table 4), indicating a decreased affinity of $p66_{N348I}/p51_{N348I}$ for NVP. Additional experiments with the subunit-specific mutant enzymes showed that the binding affinity of NVP for $p66_{N348I}/p51_{WT}$ was reduced 1.5-fold relative to WT. However, the K_{d}-NVP of $p66_{WT}/p51_{N348I}$ was similar to that of WT (Table 4).

Calculation of $k_{on\text{-}NVP}$ and $k_{off\text{-}NVP}$—The increased K_{d}-NVP for $p66_{N348I}/p51_{N348I}$ and $p66_{N348I}/p51_{WT}$ demonstrated that the mechanism of NVP resistance involves differential binding of the inhibitor. However, $K_{d\text{-NVP}}$ is an equilibrium constant ($K_{d\text{-NVP}} = k_{off\text{-NVP}}/k_{on\text{-NVP}}$) that does not distinguish whether the differences are due to a decreased rate of association ($k_{on\text{-NVP}}$) or to an enhanced rate of dissociation ($k_{off\text{-NVP}}$). To resolve the specific effects on NVP binding, we determined the $k_{on\text{-NVP}}$ and $k_{off\text{-NVP}}$ for WT and mutant enzymes (Fig. 8 and Table 4). To calculate $k_{on\text{-NVP}}$ values, we first estimated the apparent rates of NVP binding ($k_{app\text{-NVP}}$). The WT $k_{app\text{-NVP}}$ was almost ~2-fold larger than that of $p66_{N348I}/p51_{N348I}$ and comparable with that of $p66_{N348I}/p51_{WT}$. However, the $k_{app\text{-NVP}}$ for $p66_{WT}/p51_{N348I}$ was 4-fold slower than that of the WT (Fig. 8 and Table 4). We then calculated $k_{on\text{-NVP}}$ using our experimentally determined $K_{d\text{-NVP}}$ and $k_{app\text{-NVP}}$ values (Table 4). The $k_{on\text{-NVP}}$ value for WT was almost twice as high as that for $p66_{N348I}/p51_{N348I}$ (5.7×10^4 and $3.4 \times 10^4\ M^{-1}\ s^{-1}$, respectively). Interestingly, $p66_{WT}/p51_{N348I}$ displayed the largest decrease in $k_{on\text{-NVP}}$ without a significant change in $K_{d\text{-NVP}}$.

Molecular Modeling—The molecular dynamics simulations of WT and $p66_{N348I}/p51_{N348I}$ models resulted in structures that were highly similar to the starting coordinates (root mean square deviation of Cα, ~1 Å) (Fig. 9). The N348I substitution interrupted a hydrogen bond network involving the amide side chains of residues Asn-348, Gln-330, and Gln-340 (Fig. 9*A*, *top inset*). This change did not appear to significantly affect the structure of the connection subdomain. However, we observed a noticeable change at the floor of NNIBP in the molecular model of the NVP complex with $p66_{N348I}/$

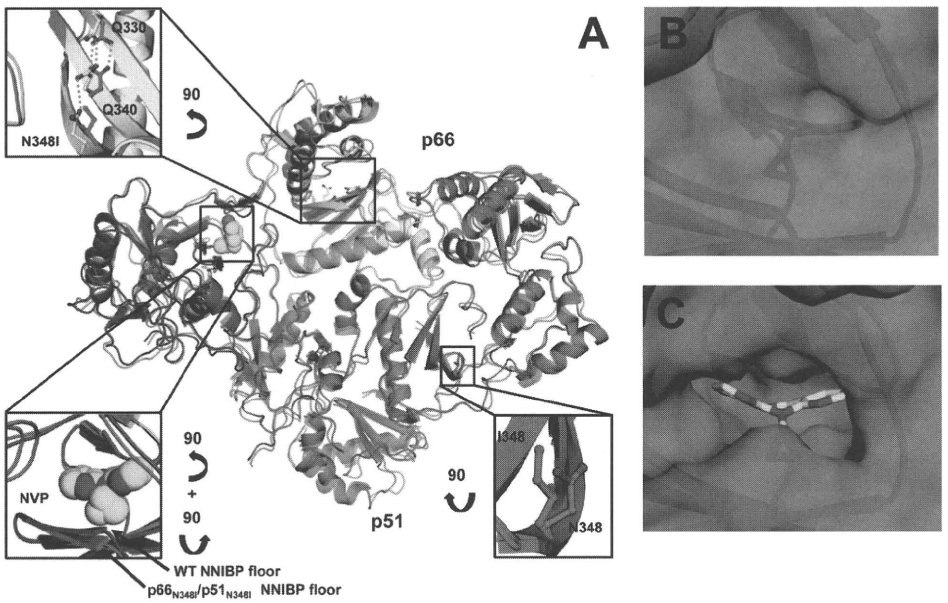

FIGURE 9. *A*, superposition of molecular models of WT RT (*multicolored* schematic; see below) and $p66_{N348I}$/$p51_{N348I}$ RT (*magenta* schematic). The molecular models were constructed using molecular dynamics simulations as described in the text. Overall, the structures are very similar (~1-Å root mean square deviation for Cα), but the mutations cause noticeable differences at the floor of the NNRTI binding pocket (indicated by an *arrow* in *inset C*). In the connection subdomain of p66 (*yellow*), the N348I mutation affects the hydrogen bond network between residues 348, Gln-340, and Gln-330. These changes appear to affect the geometry of the NNRTI binding pocket, resulting in a decreased association rate (k_{on}) of NVP (*cyan spheres*) with the N348I RT. *B* and *C*, alternate views of the NNRTI binding pockets of WT and N348I RTs. When NVP (*cyan sticks*) is bound to RT, the access to the NNRTI binding pocket is completely obstructed by the surrounding residues in the WT enzyme (*B*) but not in N348I RT (*C*). The WT RT color scheme shown in *A* is as follows: fingers in *blue*, palm in *red*, thumb in *green*, connection in *yellow*, RNase H in *orange*, and p51 in *brown*. Figures were made using PyMOL.

$p51_{N348I}$ (Fig. 9*A*, *bottom inset*, *arrow*) that may affect access to this cavity.

DISCUSSION

Previous studies have shown that changes at regions distant to the RT active sites can affect enzymatic functions (45–53). Moreover, it has been shown that NNRTI resistance can be conferred by mutation on residues of the p51 subunit alone (54). The present study with subunit-specific N348I mutants provides new mechanistic insights into how remote mutations in either subunit affect enzyme activity and drug resistance. It also establishes that, in addition to providing structural integrity (55, 56), p51 is critical in fine tuning RT enzymatic activities.

Based on simple primer extension assays, it was previously reported that WT and N348I RTs have comparable polymerase activities (31). However, our in-depth transient kinetics analysis clearly demonstrated a significantly (>3-fold) decreased catalytic efficiency for $p66_{N348I}/p51_{N348I}$. This reduction in catalytic efficiency is consistent with previous reports by us and others that HIV-1_{N348I} virus has a reduced replicative capacity (32, 33). Hence, N348I imparts a fitness cost to the virus, placing it in the special category of "desirable" mutations that would weaken the virus once acquired.

Interestingly, Ile-348_{p66} and Ile-348_{p51} each decreased catalytic efficiency, providing unexpected evidence that changes in p51 can affect the catalytic step of DNA synthesis without affecting dNTP binding (Table 1). We also found that Ile-348_{p66} and Ile-348_{p51} each enhanced processivity (Fig. 4 and Table 2). Consistent with this finding, both Ile-348_{p66} and Ile-348_{p51} slightly enhanced DNA binding affinity (Fig. 1 and Table 1). Mutation in either subunit may improve RT-nucleic acid interactions by changing the positioning and/or flexibility of enzyme regions that are in contact with DNA. Such changes may not significantly alter the $K_{d\text{-DNA}}$ but could affect proper alignment of DNA with dNTP substrates or stability of the catalytic complex. The enhanced processivity of N348I RT may also contribute to NRTI resistance as it is possible that this property could provide more opportunities for unblocking chain-terminated primers or NNRTI dissociation (38, 39). The molecular details of these effects are not yet fully understood and should be addressed by structural studies of N348I RT.

Regarding the effect of N348I on RNase H function, we confirmed a previously reported defect of $p66_{N348I}/p51_{N348I}$ in processing RNA/DNA (31, 39). Moreover, using subunit-specific mutants, we were able to demonstrate that the RNase H defect is due primarily to Ile-348_{p51} (Fig. 5), further expanding our understanding of how p51 contributes to multiple enzymatic functions.

Our reported increase in the NVP IC_{50} of $p66_{N348I}/p51_{N348I}$ is consistent with values published elsewhere (2–3-fold increase) (31, 57). These *in vitro* changes are smaller than those observed in cell-based assays for viruses harboring the same mutation (typically 7–8-fold and up to 27-fold) (31–34). Such quantitative differences between enzymatic and cell-based estimates of drug resistance are not uncommon. For example, the excision-enhancing mutations cause up to 40-fold AZT resistance in cell-based assays compared with typically ~2-fold changes observed in enzymatic assays depending on the sequence and length of the templates (longer templates provide more opportunities for inhibition) (17, 18, 58–60). During reverse transcription of the entire HIV genome *in vivo*, sequence-specific effects on inhibitor susceptibility may also contribute to stronger resistance. Importantly, the magnitude of N348I resistance to NVP *in vitro* mirrors the observed changes in $K_{d\text{-NVP}}$, indicating that the decreased binding of the inhibitor accounts for the observed resistance *in vitro*.

Our work clearly shows that the mechanism of N348I resistance to NVP involves a straightforward decrease in binding affinity for this inhibitor. Less clear is the role of RNase H in NVP resistance. Nikolenko *et al.* (38) proposed that the decrease in RNase H activity of CSMs preserves the RNA template and provides more time for NNRTIs to dissociate from the RT, resulting in the resumption of DNA synthesis and